Doctoral Thesis in Vehicle and Maritime Engineering

Experimental studies of wind and aerodynamics for wind-powered commercial ships

ULYSSE DHOMÉ

KTH ROYAL INSTITUTE OF TECHNOLOGY

Experimental studies of wind and aerodynamics for wind-powered commercial ships

ULYSSE DHOMÉ

Academic Dissertation which, with due permission of the KTH Royal Institute of Technology, is submitted for public defence for the Degree of Doctor of Philosophy on Friday the 4th of October 2024, at 09:00 a.m. in F3, Lindstedtsvägen 26, Stockholm.

Doctoral Thesis in Vehicle and Maritime Engineering
KTH Royal Institute of Technology
Stockholm, Sweden 2024

TRITA-SCI-FOU 2024:44
ISBN: 978-91-8106-045-4

Printed by: Universitetsservice US-AB, Sweden 2024

How inappropriate to call this planet Earth,
when clearly it is Ocean.

Arthur C. Clarke

Abstract

The wind is emerging again as a viable source of energy to propel commercial ships. This renewal is partially driven by new regulations aiming at cutting down the greenhouse gas emissions from the shipping industry, and partially by some actors who are willing to take a step towards this paradigm shift. Many different technological solutions have been developed or are under development since the past few years, some aiming at assisting the engines with extra wind energy and others aiming at vessels fully wind-powered.

Although sailing has existed since a long time, transitioning from a tall ship or a leisure yacht to a sailing commercial vessel is complex. Some aspects of the physics of sailing are not fully understood yet, at least not when applied to ships that are so different from existing sailing ships. Large cargo vessels will require several sails or wings, to ensure enough propulsive force. The interaction effects between lifting surfaces placed so close to each other are only partially understood, and have only been little studied when it comes to arrays of wings. The impact of the hull on the flow is something rarely studied, partly because conventional sailing boats do not have such large hulls, and partly because it only matters for fast racing yachts. The interaction effects, both wing-wing and wing-hull are studied in this thesis with different methods: a potential flow numerical code, wind tunnel experiments and with a free-sailing 7 meter long model equipped with different types of sensors.

Another question arises from the heights that wind propulsion devices reach above sea level, which are higher than any existing sailing boat, with the exception of few leisure super-yachts. The wind at these heights is partially unknown, at least offshore where ships operate. Both the evolution of wind with height and its unsteadiness have rarely been measured at heights relevant for wind propulsion. This thesis presents unique wind measurements of the Atmospheric Boundary Layer over the North-Atlantic Ocean, performed from a commercial ship in operation with a wind lidar, in an attempt to provide better knowledge of the wind conditions at sea.

In order to ensure that sailing ships will be operated in an efficient and safe manner, automation systems and control algorithms need to be developed, both for the wings and the whole vessel. These control systems will need to be able to account for all interaction effects and the unsteadiness of the wind. This thesis presents results from tests performed at sea, in real conditions, on a 7 m long scale model wind-powered car carrier, and highlights the effects of unsteadiness. The results presented in this thesis pave the way towards the development of these efficient control systems.

Throughout the thesis, different methods, with varying complexity and fidelity have been used. The results and the discussions presented in this thesis showcase the importance of mixing and combining different methods, experimental and numerical, with low and high fidelity, in order to fully understand the new questions raised by the development of sailing cargo vessels.

Keywords
Sailing, Wind Propulsion, Aerodynamics, Marine Atmospheric Boundary Layer

Sammanfattning

Vind som energikälla för kommersiella lastfartyg är på frammarsch. Utvecklingen är delvis driven av nya föreskrifter som siktar att minska växthusgasutsläpp från sjöfartsindustrin, och delvis av aktörer som är villiga att ta ett steg mot det här paradigmskiftet. Olika tekniska lösningar utvecklas parallellt, några med syftet att stötta maskinen med extra vindkraft, och andra som syftar att driva fartyget uteslutande med vindkraft.

Seglingskonsten är gammal, men att ta steget från en fullriggare eller en "vanlig" segelbåt till ett effektivt kommersiellt fartyg är komplext. Samtliga fysiska fenomen är inte helt utredda idag, i alla fall inte gällande fartyg som avsevärt skiljer sig från de traditionella. Stora fartyg har exempelvis behov av flera samverkande segel (eller vingar) för att få tillräckligt med drivkraft. Interaktionseffekter mellan dessa vingar, placerade nära varandra är bara delvis utredda och har ännu inte studerats fullt ut. Hur skrovet över vattenytan påverkar flödet runt vingarna är inte heller tillräckligt studerat. Detta delvis eftersom effekten är stor bara för kappseglingsbåtar men marginell för vanliga segelbåtar som också inte har så stora skrov som kommersiella fartyg. Interaktionseffekterna, vinge-vinge och skrovet-vinge är därför en del av den här avhandlingen, där de studeras med olika metoder: numeriskt med friktionsfri strömning i simulering, i vindtunnelförsök samt i segling med en friseglande nerskalad modell utrustad med en uppsjö sensorer.

En annan relevant aspekt som studerats är effekten av att dessa fartyg är avsevär högre än existerande segelbåtar, med undantag för några få lyxjakter. Vindförhållanden vid dessa höjder över öppet hav är faktiskt inte helt känd. Varken hur vindhastighet och riktning utvecklas med höjden eller hur vindbyar utvecklas på dessa höjder har sällan studerats i literaturen. Avhandlingen presenterar unika vindmätningar av atmosfärens markgränsskikt över Nordatlanten utförda med vind-lidar monterad på ett kommersiellt fartyg i ordinarie tjänst.

För att säkerställa att seglande kommersiella fartyg används på ett effektivt och säkert sätt ökar behovet av automatiska styr-/reglersystem samt algoritmer för trimning av vingarna samt hela fartygen. Dessa regleralgoritmer behöver sannolikt hantera, kompensera för, och effektivt utnyttja interaktionseffekter, instationära vindförhållanden och sjöförhållanden. I den här avhandlingen presenteras resultat från experiment utförda till sjöss i äkta vindförhållanden men en nedskalad 7 m lång modell av ett vinddrivet biltransportfartyg. Resultaten banar bland annat vägen för ökad förståelse för ingående fenomen samt för effektiva reglerlösningar.

Avhandlingen innehåller alltså en rad olika frågeställningar och metoder med varierande komplexitet och noggrannhet. Diskussionen och resultat visar också hur viktigt det är att i dessa tvärdisciplinära frågeställningar blanda och kombinera metoder, experimentella och numeriska, med låg och hög noggrannhet för att få svar på frågorna som utvecklingen av seglande lastfartyg kräver svar på.

Nyckelord
Segling, Vindframdrift, Aerodynamik, Atmosfärens gränsskikt,

Preface

A few years ago, while going through some boxes in the garage, I found an old notebook from school from when I was 8 years old. In this notebook, a homework “Quand je serai grand”, “When I grow up”, for which we were asked to write what we would like to work with when we grow up. Here are pictures of the three pages that I was inspired to write.

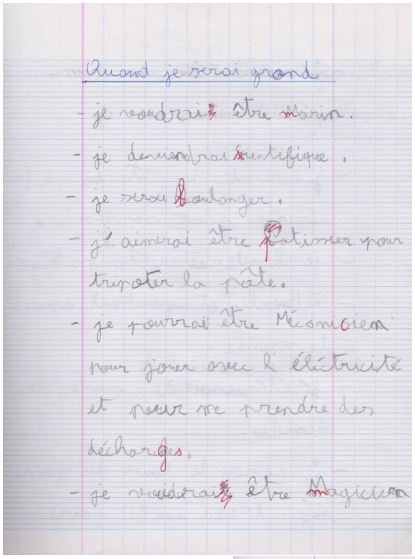

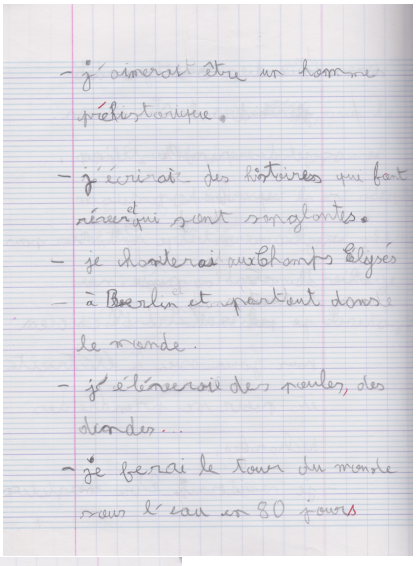

A translation could read as follows:

When I grow up

- I would like to be a sailor.
- I will become a scientist.
- I will be a baker.
- I would like to be a pastry chef, so I can fiddle with the dough.
- I could be a mechanics to play with electricity and receive electric shocks.
- I would like to be a magician.
- I would like to be a caveman.
- I will write stories that make people dream and are bloody.
- I will sing on the Champs Élysés, in Berlin and everywhere in the world
- I will raise chickens, turkeys...
- I will go around the globe underwater in 80 days
- I would like to be a volcanologist.
- I will be a naval architect.

While some of those surprise me a little, I have never been able to sing nor have I been good at magic, others are realistic: I still like to bake and to do pastry, I still enjoy fiddling with the dough, I sort of turn into a mechanics when I take care of our boat *Innis*, and I do "play" with electricity at work! I will let my friends decide how I did on the caveman part. Apart from those, I did write 24 years ago that I was going to be a scientist and a naval architect. As I wrap up my PhD thesis about sailing ships, I guess I can say that I am following a childhood dream. Some might just call that stubbornness, but I guess I am that too, so that's okay.

But most of all, this shows the support that I have always received from my parents Laurence and Thierry, who despite not being scientists themselves, always pushed me to achieve my goals, even when it meant leaving France for Sweden. I don't know how to thank them; I would certainly not be here without them. Papa, Maman, merci du fond du cœur. Je vous aime tellement. Naturally, I would also not have grown up to be who I am without my older brother and sister Hadrien and Diane, who have always been there for me, and thanks to whom I also got the joy of being an uncle of two

beautiful nieces Sarah-Lou and Lyra in the last years of my PhD and as I finish writing this thesis of a cute nephew Loukas whom I still need to meet.

I should also give credit to my grandmother Jacqueline, who was a science teacher and certainly gave me a taste for science as I was visiting the *Museum d'Histoire naturelle* in Pairs with her as a child; and to my grandfather Claude, who pushed his grandchildren to learn languages; this certainly made it easier to move to Sweden. These dreams probably would not have emerged without my grandfather Christian, who had a family summer house by the sea in Bretagne, where my parents live now, and where I could see fishing boats going out, and vessels being built (I still have newspaper cuts from when the yard *Piriou* built a supply vessel named *Ulysse* when I was six years old). But most importantly, he made a point every summer to make all his grandchildren take sailing classes at the local sailing club on the beach. I was put on an optimist when I was four years old. If he was still with us today, he would probably not understand much of what I do, but he would certainly be proud. He never did any of this on purpose, but it did help me be on track for where I am now.

More recently, my journey towards the PhD started something like 7 or 8 years ago, when I started to work with Professor Jakob Kuttenkeuleur, now my supervisor, on the autonomous sailing boat *Maribot Vane*. I don't know how to describe Jakob, so I will copy the words of my co-supervisor Mikael Razola, from his PhD thesis, "Jakob is a perpetual machine, with seemingly endless energy and a huge heart." I think this sums him up well. Working with Jakob can be intense, but also so much fun and so rewarding, I simply love it. Jakob put so much trust in me, he gave me so much freedom, I sometimes questioned if I deserved it. But as I was free, Jakob was also always there when I asked him. I really enjoy working with you Jakob, thank you so much for the opportunities you gave me! I am looking forward to continuing working together.

I wish to thank Mikael Razola as well. He has also been there since the beginning, as he was the one who made me start on the Maribot Vane project, and after, as the manager of the *wind powered car carrier* project, it was natural that he would co-supervise my PhD. I will never forget your help and calmness, the day prior to installing the lidar onboard the ship *Figaro*, when we still had to drive from Stockholm to Gothenburg and that one electronic component broke. You let me debug until I found the problem past midnight, and you let me sleep instead of sharing the driving. We didn't sleep much, but the installation went well and became an important part of my thesis! Thank you again!

On a slightly less personal note, I would like to express my gratitude to the Wallenius family and Wallenius Marine, for the support they give to research and their drive to be at the forefront of sustainable shipping. My gratitude also extends to the Berglund family, whose generous donation helped us build the 7 m model *Christiane* which became a large part of my PhD.

As I was finishing my PhD, I got the chance of visiting other universities as a guest PhD student. Thank you to Stuart Norris who welcomed me at the University of Auckland for two months and thank you to Joohyun Woo for welcoming me for two months in Busan at the Korean Maritime and Ocean University. These two experiences were very different but very enriching and I hope that we managed to create good connections that will lead to future collaborations.

I would like to thank all my colleagues from the KTH Centre for Naval Architecture for a nice work environment, for interesting conversations, work related or not, for the support we give each other. I will not try to name everyone I have good memories with, I will too likely forget some, but thank you all! I will only name two of them, Aldo Terán Espinoza, my office mate since two years and Niklas Rolleberg.

I don't fully understand what Aldo does, he doesn't fully understand what I do either, but that doesn't prevent us to discuss when we get stuck on something, and it is instead often very useful to have a novice point of view (well, at least for me, I hope it's the same for him). But more than that, it is fun to share an office with Aldo, from playing very loud *Abba* for a whole day to singing by himself with his headphones, or having to defend ourselves against the rest of the corridor, there is always a reason to have fun with Aldolito.

Finally, I want to thank Niklas for all the time we have spent together and all the help he has given me, at work but also personally. Niklas taught me so much about electronics, I would not know half of what I know without him. Niklas has always been there when I needed help to go testing a boat, be it *Maribot Vane* or the 7 meter model *Christiane*, he simply never said no. We have been together at sea in the middle of the night, watching over *Vane*. Niklas had to explain to the Sea rescue society, who came with two boats and a helicopter, that no-one fell from *Vane*, since it is an autonomous boat. We have been stopped by the coast guard in the middle of a channel when it was dark and cold on an October night, towing back *Christiane* after several days out at Askö. But also, when Chiara and I were in London for a conference, Niklas was there to go and sign the contract for us to buy our apartment, and he was there again three months later to help us move until 1 a.m. because I booked a too small van. Thank you so much Niklas!

Apparently, there is one more of my childhood dreams that I partially followed. My stories may not make people dream and they are not bloody, but I do have a tendency to write long... So it is time to finish this long preface by thanking Chiara, my girlfriend, my friend, my life partner and also colleague. Let's be realistic, I would have probably finished my PhD a year or two ago if she had not been there. Thanks to her, I learned to avoid working too late every day and weekends; I learned that I should also enjoy my social life rather than putting it on hold for work, even if I love my work. Thank you for that. But at the same time, thank you for being there for me. Thank you for your support also at work, via long technical discussions, by proof reading my papers, helping me prepare experiments, even when it needed to be done in a rush late a night the day before because the ship is not going to wait for us or because winter is approaching and if I didn't go testing before it froze, I had to wait several months to do my experiments. You bring me so much joy, I just need to look at you and all my doubts disappear. Je t'aime immensément!

Ulysse Dhomé
Stockholm, September 2024

List of appended papers

Paper A

Ulysse Dhomé, Jakob Kuttenkeuler and Antonio Segalini, 2024, *Observation of the Atmospheric Boundary Layer over the Atlantic and its effects for wind propulsion.*, Submitted to the Journal of Wind Engineering and Industrial Aerodynamics, under review.

Paper B

Laura Marimon Giovannetti, Ulysse Dhomé, Karolina Malmek, Adam Persson and Chiara Wielgosz, 2022, *Multi-wing sails interaction effects*, SNAME 24th Chesapeake Sailing Yacht Symposium, Annapolis, USA.

Paper C

Ulysse Dhomé, Antonia Hillenbrand, Jakob Kuttenkeuler and Niklas Rolleberg, 2024, *Unsteady pressure measurements at sea on the rigid wings of a model wind propelled ship. Part A: Measurement system development.*, paper submitted to Ocean Engineering.

Paper D

Ulysse Dhomé, Antonia Hillenbrand, Jakob Kuttenkeuler and Niklas Rolleberg, 2024, *Unsteady pressure measurements at sea on the rigid wings of a model wind propelled ship. Part B: in-situ aerodynamic performance measurements.*, paper submitted to Ocean Engineering.

Paper E

Ulysse Dhomé, Cynthia El Khoury and Jakob Kuttenkeuler, 2023, *Evaluation of the flow state over a rigid wing-sail through tell-tale detection using computer vision*, The 6th International Conference on Innovation in High Performance Sailing Yachts and Wind-Assisted Ships (INNOV'Sail 2023), Lorient, France.

Publications not included in the thesis

Adam Persson, Da-Qing Li, Fredrik Olsson, Sofia Werner and Ulysse Dhomé, 2019, *Performance prediction of wind propulsion systems using 3D CFD and route simulation.*, RINA Wind Propulsion Conference 2019, London, U.K.

Karolina Malmek, Ulysse Dhomé, Lars Larsson, Sofia Werner, Jonas W. Ringsberg, and Christian Finnsgård, 2020, *Comparison of two rapid numerical methods for predicting the performance of multiple rigid wing-sails.*, The 5th International Conference on Innovation in High Performance Sailing Yachts and Sail-Assisted Ship Propulsion (INNOV'Sail 2020), Online.

Ulysse Dhomé, Jakob Kuttenkeuler, Mikael Razola, and Antonio Segalini, 2020, *Preliminary results on measurements of the atmospheric boundary layer over the atlantic.*, The 5th International Conference on Innovation in High Performance Sailing Yachts and Sail-Assisted Ship Propulsion (INNOV'Sail 2020), Online.

Antonia Hillenbrand, Ulysse Dhomé, Jakob Kuttenkeuler, and Mikael Razola, 2021, *Development of a 1:30 scale sailing model of Oceanbird.*, RINA Wind Propulsion Conference 2021, London, U.K.

Division of work between authors

Paper A

A discussion between Dhomé and Kuttenkeuler led to the decision of realising the measurement campaign. Kuttenkeuler ensured the financing and procurement of the wind lidar and the rest of the equipment. Dhomé prepared the sensors and coded the data acquisition system, installed the equipment on the ships and ensured its continuous functioning. Data curation and post processing was performed by Dhomé. Segalini had an active role in deciding upon the methodology. The main manuscript was written by Dhomé, with Segalini and Kuttenkeuler reviewing and editing it.

Paper B

Marimon Giovannetti was the principal investigator of the experimental campaign. Dhomé had an active role in the discussions that led to the realisation of the experiments, which were not initially planned in the scope of the research project. The experiments planning was done by Marimon Giovannetti and Dhomé with the help of Malmek. All authors participated in the experiments. The manuscript was mainly written by Marimon Giovannetti, except for the results which were shared between Marimon Giovannetti, Dhomé and Wielgosz.

Paper C and D

The idea of using pressure sensors for the purpose of the papers came from discussions between Kuttenkeuler and Dhomé. Paper C is based on experiments done for the master's thesis work of Hillenbrand, under the supervision of Dhomé and Kuttenkeuler. The implementation of the sensors in the boat was done by Dhomé and Hillenbrand for the experiments in Paper C and by Dhomé for the experiments in Paper D. The software was written by Rolleberg, Hillenbrand and Dhomé. The methodology and the choice of experiments arose from discussions between Dhomé, and Hillenbrand for Paper C, while Dhomé alone prepared, executed and processed the experiments for Paper D.

Paper E

The idea of the paper came from Dhomé. The original computer vision algorithm was implemented by El Khoury as part of an internship supervised by Dhomé and was modified by Dhomé for the experiments in the paper. The

implementation of all cameras on the boat and the experiments were performed by Dhomé. The manuscript was written by Dhomé, with comments and proof-reading by Kuttenkeuler and El Khoury.

Contents

List of Figures

Chapter 1

Introduction

1.1 Need and incentives for decarbonisation of the shipping sector

Nowadays, about 90% of the goods are transported at some point at sea. This makes international maritime shipping responsible for about 3% of the global greenhouse gas emission worldwide [17]. In line with the Paris agreement, the International Maritime Organisation (IMO) adopted goals for the reduction of emissions from shipping in 2023 during the 80th session of the Maritime Environment Protection Committee (MEPC 80). Compared to the levels of 2008, the emissions from shipping need to be lowered by at least 20% in 2030 and at least 70% in 2040, striving for 30% and 80% respectively, and should reach net-zero by 2050.

In order to meet the targets set by the IMO, new sources of energy for the propulsion of ships need to be used. Not the easiest to develop, but nonetheless a promising way is to use the wind, either as an assistance, to reduce the fuel consumption, or as a primary source of propulsion. The sector is expanding rapidly, as shown in the last edition of the Loyd's Register energy efficiency retrofit report [39]: between 2018 and 2023, 29 vessels had Wind Propulsion Systems installed, whereas in 2024 alone, counting installations and confirmed ordered, 72 ships will be retrofitted. Most of these projects only concern retrofit on existing vessels of solutions for wind assistance. Only few projects at the moment aim at fully sailing vessels.

Different technological solutions are being developed, the main ones being rigid wings, soft sails, Flettner rotors, suction sails and kites. These technologies all have advantages and drawbacks, and have different performance in different conditions. The variety of technical solutions matches the variety of ships, which exist in all sorts of sizes and are going on all sorts of routes.

1.2 The wind Powered Car Carrier and Orcelle Horizon projects

The ship design company Wallenius Marine started a road map towards zero-emission shipping about 20 years ago, with a vision to harness wind but also wave energy to power the ships of the future in the project *ZERO* (Zero Emission ROro) [42]. On this path, Wallenius Marine has been a leader in reducing the footprint of their vessels, with ballast water treatment solutions (Pure Ballast, a joint company with Alfa Laval) but also high efficiency hull design and new fuels, such as the design of the worlds first LNG powered Pure Car and Truck Carrier (PCTC) for UECC in 2016 and the HERO class of PCTC in 2018, which was the most energy efficient PCTC at this time.

After an internal prestudy, Wallenius Marine started the wind Powered Car Carrier (wPCC) project in 2019, in collaboration with SSPA (now RISE Maritime), a Swedish maritime research centre, and KTH Royal Institute of Technology, a leading Swedish engineering university, with the financial support of the Swedish Transport Administration, *Trafikverket*. The three-years project aimed at raising the technology readiness level for the development of a wind-powered vessel with the goal of reducing the emissions by 90% compared to conventional car-carriers. The research project included many different aspects, ranging from logistics, risk analysis, aerodynamic and hydrodynamic performance and method development, as well as routing. The research and the commercial projects led to the presentation in 2020 of the *Oceanbird* concept and in early 2021 of *Orcelle Wind*, the first vessel of the *Oceanbird* concept to be ordered by the Wallenius-Wilhelmsen shipping company. Later in 2021, Wallenius and Alfa Laval created the joint venture *AlfaWall Oceanbird*, which develops the wingsail solution and unveiled a new wing design.

(a) The wPCC concept. © Wallenius Marine. (b) The Orcelle Wind concept. © Wallenius-Wilhelmsen.

Figure 1.1: Artistic renderings of the wPCC and the Orcelle Wind concepts.

After the end on the wPCC project, a European project within the Horizon Europe framework called *Orcelle Horizon* started at the beginning of 2023. It is a continuation of the wPCC project, but with an even larger scope, since it includes seven more participants apart from Wallenius Marine, RISE and KTH, ranging from Wallenius-Wilhelmsen, other european universities, regulators with the participation of DNV and even cargo owners who will ship their cargo on the *Orcelle Wind* vessel.

The research presented in this thesis started with the wPCC project, with a focus on aerodynamics and control of such wind-powered vessel. Others aspects of the research performed at KTH Centre for Naval Architecture within the wPCC project are risk assessment, performance prediction and weather routing. In the *Orcelle Horizon* project, the focus is on methods for aerodynamic performance evaluation but also on sensing, wing trimming strategies and control algorithms development.

1.3 New challenges and the need of new methods to tackle them

The development of such ships creates new challenges and calls for new methods to tackle them. This thesis presents several of those challenges and ways to solve them.

A major challenge comes from the sailing itself. The crew cannot be expected to be trimming the sails constantly like it was on old merchant ships. First of all, there would be a lack of knowledge in how to do so. Sailors use a lot their senses to know how to trim a sail, particularly on yachts, but also on tall ships: Did the wind vary? Does the boat roll or pitch? Is the moment on the rudder too large? Do the sails flap? Are the tell tales flying? How could a sailor feel any of these sensations on a more than 200 m long ship, weighing more than 30000 tons? How could they see tell-tales 40 m above the deck? How can they feel the rudder when it goes through electric and hydraulic systems?

More importantly, such ships and the flow around them will be so complex that a human would hardly be able to harness all its potential. At the latest stage, the *Orcelle Wind* concept has, for example, a dozen possible degrees of freedom: six wings with each two possible rotations, rudders, and an engine (when motor-sailing). How could a human being be able to optimise all of those to make the best use of the vessel? Maybe even more important: how would the crew be sure that these settings are safe and that they don't risk putting the vessel in danger because of excessive forces, loss of manoeuvrability or excessive boat motions?

Going away from the ship, the commercial aspects put hard constraints on its usage, since the goods need to be delivered within a specific time

frame. How would the captain be able to decide on the best route to follow given the variability of the wind around the globe? Even with good quality weather forecasts, the optimal route can only be chosen knowing precisely how the ship will perform in different wind and sea conditions and sailing at different wind angles; there are simply too many factors to take into account for a human to do such a task in an optimal way.

All the above mentioned show the need for automatic, efficient and safe control systems, for the wind propulsion units, for the vessels, but also at a higher level with optimal routing. Unfortunately, this is easier said than done, and this need for control algorithms creates new challenges as well.

For weather routing, an important aspect is how reliable and accurate the weather forecast is, but this is a question for meteorologists, not naval architects. What concerns the ship more is that a routing will only be as good as the vessel performance prediction is. In turn, a velocity prediction program will only be as good as its hydrodynamic and aerodynamic models.

But again, how good is the aerodynamic model if the interaction effects between the wings and the influence of the hull are not fully understood? How good will it be, if the wind profile used in the prediction is not what actually happens out in the ocean? Even with good knowledge of the interactions and of the wind by themselves, what happens when they are combined and a ship sails in real, unsteady wind conditions? And finally, while we are out there at sea, how do we measure all these? How do we know that this wing produces this much force, but that other one generates that much? How do we know what the wind conditions are right now?

These are questions that this thesis tries to shine light on and hopefully, partially answers. Most of these questions are complex, involve many aspects, and could be solved in many ways. In this thesis, mostly experimental approaches were chosen, some traditional like wind tunnel testing, and other less common, with a free-sailing ship model and *in-situ* wind measurements from a commercial vessel. These methods have strong arguments for them and allow to derive important results, but they are nonetheless also flawed and it is only when combined, also with other methods, that they enable to fully answer all of the above questions.

One could wonder why there is a need for aerodynamic research, when airplanes have been around for a long time and plenty of research has been done. After all, a wingsail is not much more than an airplane wing put vertically, isn't it? To some extent yes, but there are some major differences which create the need for new research in the field. A very important, and obvious difference between an airplane and a sailing vessel is the speed. While a typical airliner travels at speeds about 230 m/s, a sailing cargo vessel like the wPCC is expected to travel around 6 m/s. Typical wind speeds near the earth surface are around 7-10 m/s, and somewhere around

40 or 50 m/s at the cruising altitude of an airliner, therefore, for an airplane, regardless of the direction of the wind, the apparent wind will always come from straight ahead, while on a sailing vessel, the wind might be blowing from any direction. On an airplane, the geometrical position of the wing is what determines the force developed once in the air, while for a ship, the wings need to be adjusted to account for the wind. The second important aerodynamic difference between a sailing ship and an airplane is that planes typically only have one wing, two when counting the tail, which is small in comparison, and placed very far downstream. Therefore, the interaction between the wing and the tail is not comparable to the interactions between lifting surfaces on a ship, where, to provide sufficient thrust, they need to be large and placed in the vicinity of each other. These differences explain why there is a lack of literature about interacting wings and a need for new methods to explore these effects.

The thesis is organised as follows: in Chapter 2, a brief overview of wing and sailing aerodynamics is given, in an attempt to give readers from a different field the key concepts used in the thesis. Chapter 3 gives a short presentation of the technical aspects of the wPCC test case, followed by descriptions of the different methods used throughout the thesis: a numerical potential flow simulation method, a wind lidar measurement campaign, wind tunnel tests and finally a free-sailing 7 meter long scale model of the wPCC. These different methods are then combined to present results that help understanding the wind in Chapter 4, understanding several interaction effects in Chapter 5, and the benefit of efficient trimming strategies in Chapter 6. The results are followed in Chapter 7 by some discussions and opening towards future work. Finally, Chapter 8 gives short summaries of the appended papers, showing their contributions to the field.

Chapter 2

Basic aerodynamics and fundamentals of sailing

This chapter serves as an introduction to the notions of wing aerodynamics and sailing that are discussed in this thesis. Many renown references exist and should be consulted for further information. For what concerns wings and aerodynamics, some famous references are the books by Abbott [1] or Anderson [4]. For a more accessible reading, the "Beginners guide to Aeronautics" [9] from the Glenn research centre at NASA is a good reference. For literature about sailing physics, a must read is the book by Fossati [18].

2.1 Basics of wing aerodynamics

2.1.1 Geometry and force generation

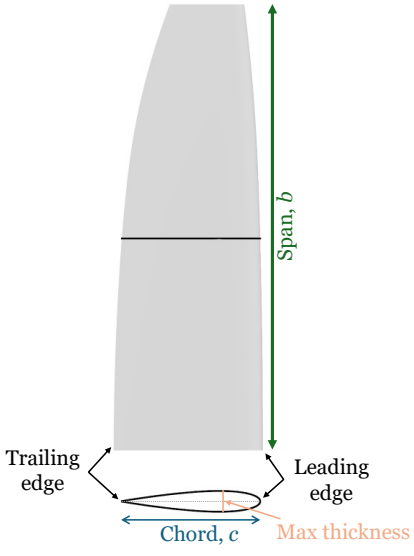

Figure 2.1: Representation of a wing and its airfoil profile.

An airfoil is an aerodynamically shaped section, which when put in an airflow, is designed to generate a substantially larger lift force, perpendicular to the flow, than a drag force, aligned with the flow. A wing is the 3D extension of an airfoil and consists in an extrusion of airfoil profiles. Figure 2.1 shows an example of a wing and its airfoil profile, with some important terms. The leading edge of the wing or the profile is the most curved part, that is hit by the wind first, and the trailing edge is the opposite point of the profile, where the flow "exits". The chord length or simply chord represents the length of the straight line connecting the leading and trailing edges. An airfoil is called symmetric if the upper and lower surfaces are symmetric, and is called asym-

metric, or cambered if they are not. For an asymmetric profile, the camber line is the line constituted by the points halfway between the upper and lower edges. For symmetric profiles, the chord and camber line coincide. Asymmetric profiles are typically what form the wings of airplanes; they usually generate higher lift than symmetric profiles, but only in one direction. A traditional soft sail is a kind of asymmetric profile, but because it is flexible, can deform to one side or the other, allowing the boat to sail in any direction. In this thesis and in the wPCC project, rigid wings are considered, therefore they need to be symmetrical to allow the vessel to sail in any direction. An airfoil can have any shape, but a number of "families" of airfoils exist and are typically used in engineering applications. A very common family is the so-called NACA 4-digit series. The first two digits refer to the maximum amount of camber and its chordwise position, and the last two relate to the maximum thickness of the profile. The symmetric profiles from this series are denoted NACA ooXX.

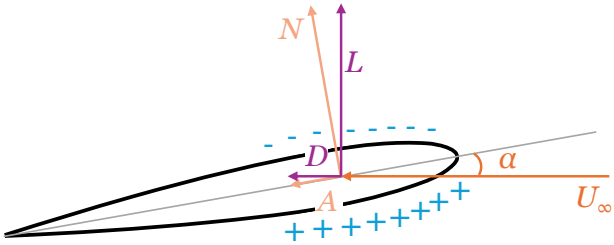

Figure 2.2: Schematic representation of the forces acting on an airfoil.

Figure 2.2 shows a sketch of the forces acting on an airfoil profile when subjected to an incoming flow. In this case, a NACA symmetric profile is shown with an angle of attack $\alpha = 10°$, defined as the angle between the chord line and the incoming flow. The incoming wind, noted U_∞ comes from the right. This generates a lift force L, which is by definition perpendicular to the flow and a drag force D, parallel to the flow. Another way to decompose the forces is in the normal force N, perpendicular to the chord line and the axial force A, aligned with the chord. Note that the magnitude of the drag force is exaggerated for better visualisation.

The exact physical phenomenon that is at the origin of the lift force is not consensual, with many popular theories that are knowingly wrong, however a consensus nowadays is that the presence of the airfoil deflects the flow, which means the flow has to exert a force of opposite direction and same magnitude on the airfoil, by application of Newton's third law. An important impact of the lift generation is that it results in the velocity on the upper surface to increase, hence in application of Bernoulli's principle, the pressure

decreases, and on the lower surface, the velocity decreases and the pressure increases. The upper surface is often referred to as the *suction side* and the lower one as the *pressure side*. This is illustrated in Figure 2.2 by the minus signs on the suction side and the plus signs on the pressure side.

At the extremities of a wing, the air is free of obstruction, thus because of the pressure difference between the suction and pressure sides, an airflow from the high pressure towards the low pressure area appears, which leads to the formation of tip and root vortices. These vortices have a detrimental effect on the performance of the wing, by decreasing the lift and increasing the drag, by adding what is called the *induced drag*. The rest of the drag is called the form drag, which is due to the skin friction and to the shape of the profile.

Two measures are typically taken to reduce the induced drag, one consists in limiting the size of the tip vortex by adding winglets like on many airplanes, or by tapering the wing towards the tip. The ratio between the tip chord and the root chord is called the taper ratio. The other one consists in having the most slender possible wing. The aspect ratio is the measure of slenderness, it is defined as the division of the square of the span b by the area S of the wing, $AR = b^2/S$. The wing depicted in Figure 2.1 has a taper ratio of 0.5 and an aspect ratio of 3.47.

Apart from the airfoil profile, the factors that affect the lift and drag generation are the wind speed U_∞ and the air density ρ. In order to compare the ability to generate lift and the amount of drag of an object, the forces are usually reduced to force coefficients, defined as

$$C_L = \frac{L}{\frac{1}{2}\rho U_\infty^2 S}, \tag{2.1}$$

for the lift, and

$$C_D = \frac{D}{\frac{1}{2}\rho U_\infty^2 S}, \tag{2.2}$$

for the drag.

The term $q = \frac{1}{2}\rho U_\infty^2$ is often referred to as the dynamic pressure. The coefficients are function of the angle of attack α, and are typically represented in lift and drag curves as shown in Figure 2.3.

Figure 2.3 shows the evolution of the lift and drag coefficients obtained from wind tunnel experiments with the wing depicted in Figure 2.1. The lift coefficient is represented by plain lines and should be read on the left axis, while the drag coefficient is shown by the dashed lines and is read on the right axis. For small α, the lift curve is linear, typically up to around $\pm 10^\circ$, and starts curving until it reaches a maximum, called stall. After stall, the lift coefficient drops significantly, more or less abruptly depending on

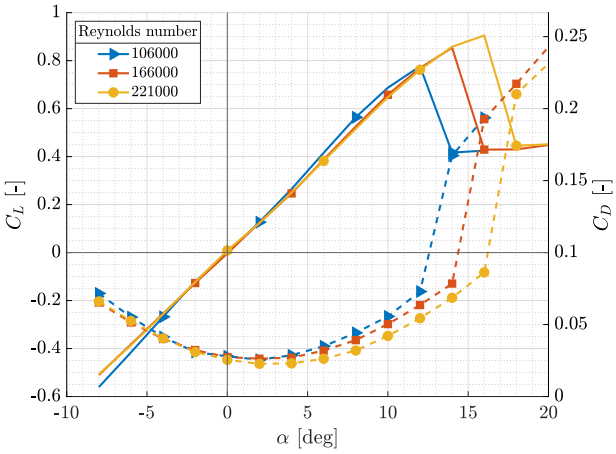

Figure 2.3: Example of lift and drag curves.

the profile and conditions. The drag curve shows a slow increase as the angle of attack is increased, until after stall when a large jump appears and the drag increases substantially. The angle at which the maximum lift is reached is called the stall angle. Stall is the phenomenon when the flow cannot follow the curvature of the airfoil anymore and it separates from the surface. Another point of interest is the zero-lift angle, explicitly the angle at which $C_L = 0$. In Figure 2.3, since the profile is symmetric, the angle of zero lift is $\alpha = 0°$.

As already mentioned, the forces acting on a wing depend on the viscosity, but also on the inertial effects. The balance between the inertial forces and the viscous forces is given by the Reynolds number, defined as

$$Re = \frac{\rho U_\infty l}{\mu} = \frac{U_\infty l}{\nu}, \tag{2.3}$$

with l a reference length, μ the dynamic viscosity and ν the kinematic viscosity of the fluid. For small Re, the viscous effects are particularly important and cannot be neglected, whereas for large Re they can be neglected as the flow only depends on inertial effects. The reference length l depends on what is considered. In the case of a wing, the Reynolds number is commonly based on the chord length, while for Boundary Layer flows, the reference length is usually the length of interest along the surface from its origin. The importance of the Reynolds number lies in the fact that if two flows have the same Reynolds number, the flow physics is the same and the outcomes are the same. This is the basis for wind tunnel testing, where the flow over a large wing can be mimicked at small scale by increasing the wind speed or decreasing the kinematic viscosity.

An important effect of the Reynolds number on the performance of a wing is showed in Figure 2.3, where the lift and drag curves are showed for $Re = 106000$, $Re = 166000$ and $Re = 221000$. At these moderate values of Reynolds number, the stall angle and maximum lift coefficient increase with increasing Re. For higher Reynolds number, eventually this effect disappears, with the stall angle and maximum lift coefficient reaching a constant value. However, there is no clear value of Re above which this happens, but a common rule of thumb is to consider that the variations should disappear for $Re > 10^6$.

An aspect that is not showed in Figure 2.3 is the stall hysteresis phenomenon that can be present. This is characterised by the fact that once the wing is stalled, if the angle of attack is reduced, the lift coefficient does not follow the same curve as when the angle was increasing, but instead has much smaller values. The curve obtained with decreasing angle of attack becomes again the same as the one for increasing only if the angle of attack is decreased enough, typically at an angle smaller than the stall angle by a few degrees, forming a so-called hysteresis loop.

2.1.2 Boundary layers

One reason for the dependency on the Reynolds number is the behaviour of the boundary layer. The boundary layer is a thin layer right above a surface in which the velocity varies: at the surface, the fluid velocity is zero because the air molecules stick to it, then the velocity increases gradually throughout the boundary layer until it reaches the free-stream velocity at its edge. Figure 2.4 shows an example of the boundary layer measured on the floor of the L2000 wind tunnel at KTH. Compared to the boundary layer on a wing, the thickness is much higher here because the boundary layer has grown over several meters.

Inside of the boundary layer, the viscous effects are predominant. Boundary layers are classified as laminar or turbulent depending on the flow state. The flow in a laminar boundary layers is “smooth”, with little variations, while in a turbulent boundary layer, it is chaotic and swirling. Laminar boundary layers are less thick and create less skin friction drag than turbulent ones, however they are naturally unstable, and are prone to detach from the surface more easily than turbulent ones. On a wing at moderate or high Reynolds number, the boundary layer is laminar near the leading edge and transitions to a turbulent boundary layer at the transition point which varies with Reynolds number. Since turbulent boundary layers are more stable, it is sometimes favoured to force the transition with the help of turbulence generators or surface roughness, to prevent separation. The value of Reynolds number above 10^6 mentioned above is considered as a

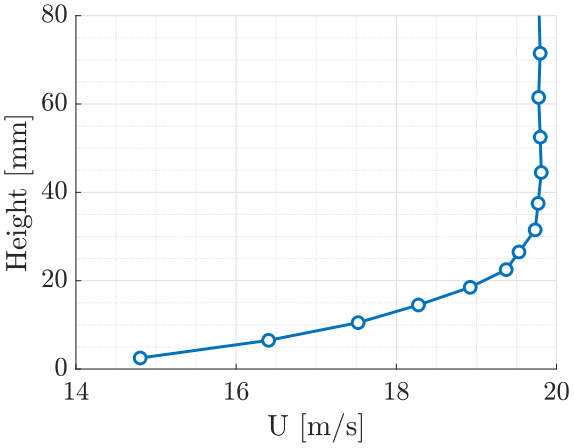

Figure 2.4: Example of a boundary layer developing on the floor of a wind tunnel.

threshold above which the flow does not depend on Reynolds number anymore because the boundary layer over the wing is likely fully turbulent at this stage.

2.2 Fundamentals of sailing

2.2.1 Definitions

Figure 2.5 shows the main angles and wind-related definitions. The ship has a heading Γ_{th} and a course over ground Γ_{cog}, which differ by the leeway angle λ, due to currents and the side force generated by the hull and the wings under the wind influence. The speed over ground SOG is the speed of the vessel in the direction of Γ_{cog} which differs from the boat speed in the presence of leeway.

The main parameter that influences the behaviour of a sailing boat is the wind angle. The true wind direction Γ_{twd} is the direction where the wind is blowing from with respect to North. The angle between the true wind and the vessel speed vector is the true wind angle β_{tw}, but what affects the sailing behaviour is the apparent wind, which is the resultant of the true wind and the speed of the vessel. The apparent wind angle β_{aw} is defined as the angle between the ship's heading and the apparent wind and is the main parameter that affects the performance of a sailing vessel.

The vectors of true wind, apparent wind and vessel speed, shown in blue, orange and red respectively in Figure 2.5, form what is referred to as the *wind triangle*. The apparent wind is the wind resulting from the vector summation

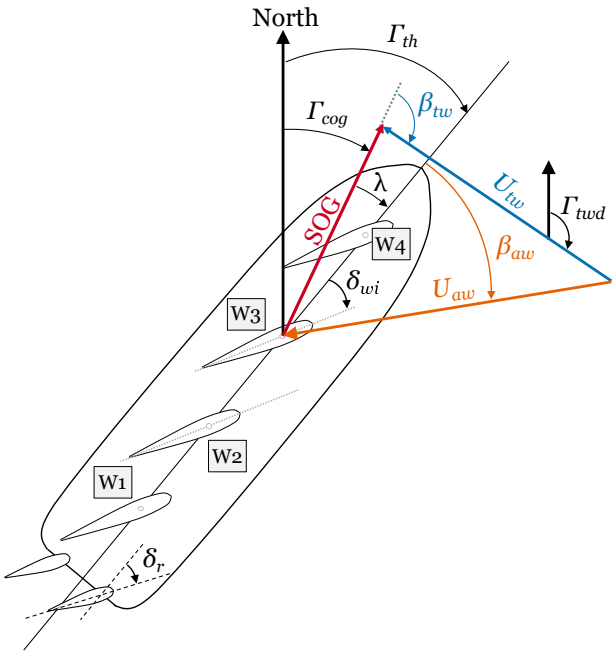

Figure 2.5: Angles and wind definitions.

of true wind and boat speed. From this triangle, one can easily understand that and increase in SOG with constant wind speed, due to better trimming for example, leads to a smaller β_{aw} and instead, an increase of wind speed U_{tw} with constant SOG leads to a larger apparent wind angle. An aspect discussed further in this thesis, is that the wind speed increases with height in the Atmospheric Boundary Layer. The effect of this speed increase is that from the base of a mast to the top, β_{aw} increases, leading to *twisting* of the wind.

Note that all authors do not agree on the definition of true and apparent wind angles. Here, the definitions might seem not rigorous because the true wind and apparent wind are based on different references. This choice is based on practical aspects: the apparent wind is typically measured by an anemometer fixed on the ship, therefore using the ship's centreline as a reference is the most obvious choice. If the apparent wind angle is defined with respect to the vessel speed vector instead of the centreline, it becomes difficult to compare cases, especially when looking at the impact of the hull or the wing-wing interaction effects, thus using the centreline as a reference makes comparisons more understandable. Since the wind triangle really

originates from the speed over ground of the ship, the true wind would not be correctly estimated if only the longitudinal boat speed component was used, therefore it is defined with respect to the ship speed over ground vector.

2.2.2 Force balance

Figure 2.6 shows the aerodynamic forces that are present on a wind-powered vessel with multiple wings as seen in a horizontal plane. As shown in Figure 2.2, each wing generates a lift force L_{wi} perpendicular to the apparent wind and a drag force D_{wi} aligned with the flow. The sum of the forces from each wing and from the hull result in a total aerodynamic force F, which can be decomposed in a thrust force F_x, aligned with the ship and a side force F_y, perpendicular to the ship. The relative strength of the forces between the wings leads to a varying location of the total force, at the aerodynamic Centre of Effort, denoted CoE aero in Figure 2.6.

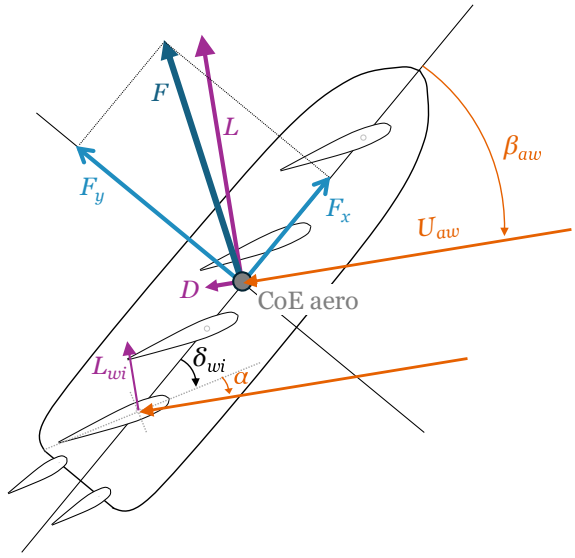

Figure 2.6: Schematic of the aerodynamic forces on a sailing vessel.

They are not represented in Figure 2.6, but as a result of the aerodynamic forces, hydrodynamic forces are generated by the hull and rudders, which are of same magnitudes but opposite directions as the aerodynamic forces when sailing on a straight course at constant speed. The hydrodynamic forces are applied at the Centre of Lateral Resistance (CLR), whose position

is modified by the rudder deflection to ensure that no yaw-moment is created by the distance between the CoE and the CLR. This results in the rudders being almost always deflected to a constant value, as shown in Figure 2.6, when sailing on a straight course.

Here only the horizontal forces are discussed, but similar effects appear in the vertical planes passing by the centreline and the transversal axis of the ship. The side force generates a heeling moment and the thrust generates a pitching moment which are statically compensated by the shifting of the centre of buoyancy.

2.2.3 Wing trimming and vessel performance

In Section 2.1, we showed that the maximum lift of a wing is generated at the stall angle, around 10° to 20°, depending on the profile and the Reynolds number. In order to maximise the speed of a sailing vessel, the sails, or wings should be rotated near the stall angle. However, as a consequence of the large loss of lift after stall and the possible presence of hysteresis, it is favourable to trim the wings at an angle smaller than the stall angle in order to accommodate for wind variations. In the example of Figure 2.3, for the Reynolds number 221000, the stall angle is 16°, with $C_L = 0.9$ and at $\alpha = 18^\circ$, after stall, the lift coefficient is divided by two, with $C_L = 0.45$. At $\alpha = 12^\circ$, $C_L = 0.75$, thus only about 17% smaller than the maximum. It would therefore be beneficial to trim this wing around $\alpha = 12^\circ$ or a bit higher, allowing for a few degrees of margin before stall, but maintaining a high lift level.

The trimming angle described here is relative to the wind, but a vessel sails with different apparent wind angles, therefore, the angle of the wings and the resulting total force are largely varying. Figure 2.7 shows the different point of sail that a sailing boat can sail at. Only the main directions are showed, but many subdivisions exist. When the wind comes from the starboard side of the boat, the vessel is on "starboard tack" and similar on port. The blue area in the figure shows the angles at which a boat cannot sail because the resulting force does not generate thrust. It is here showed as 45° to the wind to simplify, but this value depends on the ship and sails. For a vessel with rigid wings, it is typically possible to sail higher towards the wind than with soft sails which cannot withhold their shape when sailing too high. *Close hauled*, sometimes simplified as *upwind* in this thesis, is when the boat sails as close as possible to the wind. *Beam reach* is when the wind comes at a right angle with the ship. All angles past beam reach are often referred to as *downwind* sailing, but specifically when $\beta_{aw} = 135^\circ$, it is called *broad reach*. The examples in Figures 2.5 and 2.6 show the a vessel close hauled on starboard tack.

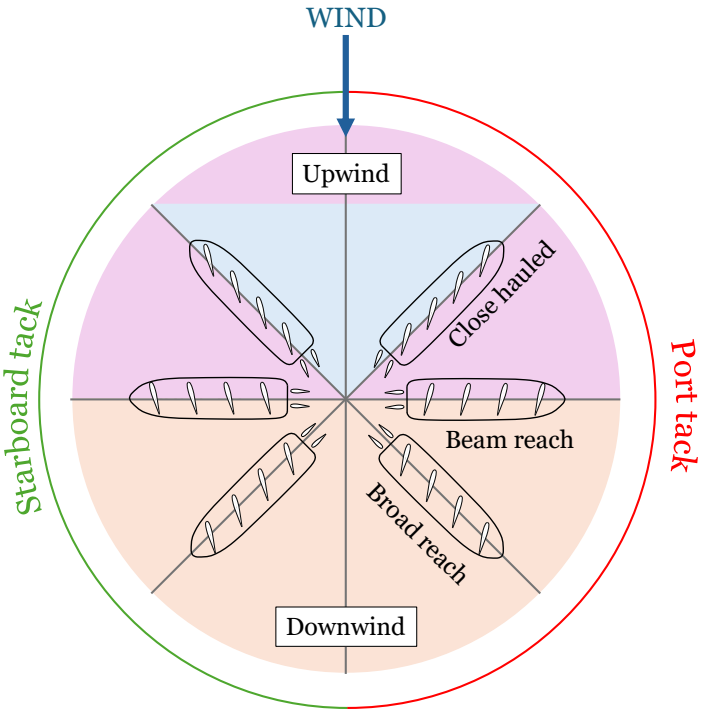

Figure 2.7: Point of sail: terminology of different apparent wind angles.

Figure 2.7 also shows an example trimming of the wings of a wind-powered vessel like the wPCC concept: at all apparent wind angles, the wings have the same angle to the wind, close to the stall angle as described above. One result arising from this is that the direction of the force varies tremendously with the apparent wind angle. Upwind, as shown in Figure 2.6, the total force is mostly directed towards the side of the ship in the same direction as the wind, leading to a large side force. On a beam reach instead, the force is almost aligned with the ship direction. These comments would apply the same to a conventional sailing vessel with soft sails, but the broad reach case is instead very different. On a broad reach, like upwind, the force is largely directed towards the side of the ship, but contrary to the close hauled case, the side force is directed to windward (towards the wind). With conventional soft sails, for practical reasons, they cannot be turned more than about 90° from the boat's centreline. When sailing downwind, soft sails are therefore trimmed to generate the most possible drag instead of the most lift as they do upwind (with the exceptions of spinnakers which can be used for both lift and drag generation). With rigid wings able to

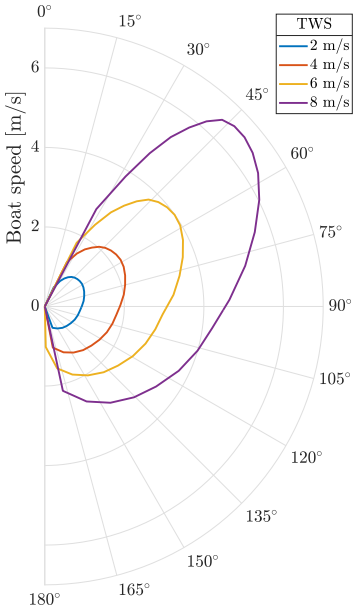

Figure 2.8: Example of a polar plot of a boat.

rotate $360°$, as in the wPCC concept, the wings can always be trimmed for maximum lift. If the wings are only trimmed to generate lift, the vessel is not able to sail straight downwind, since almost all of the force would be sideways, thus generating another "no-go zone" downwind.

By combining an hydrodynamic and aerodynamic models of a ship in a Velocity Prediction Program, it is possible to obtain a *polar* of the vessel, showing the boat speed that can be attained for different true wind speeds and varying apparent wind angle when optimising the trimming, as represented in Figure 2.8. The example in this figure is based on an early stage of the wPCC concept, and shows that despite the less favourable force direction the maximum attainable speed is when sailing upwind for this vessel. This is again rather different than a conventional sailing boat which are typically faster downwind, around broad reach.

Such polar of the boat are particularly important at a design phase, since they give an overview of the performance of a ship, all the way up to the financial aspects of choosing a specific type of wind propulsion device [24]. They are also necessary for routing and can be used in control systems.

Chapter 3

Methods and experimental resources

In this thesis, the results arise from different methods, and very different experimental campaigns and measurement systems. The results in this manuscript are presented by theme, not by papers or experiments. For ease of comprehension throughout the thesis, the methods and experimental means are briefly presented in this chapter. More details are available in the appended papers.

The first section describes the geometry of the wPCC project design, which was used as a test case for all aerodynamic studies. The second section is about a numerical code that was used at the beginning of the research project; the third section presents a campaign to measure the offshore wind in the North-Atlantic Ocean. In the fourth section, a wind tunnel campaign is shown and finally the last section presents the free-sailing 7 meter model that was developed and built as part of the thesis.

3.1 The wPCC test case

The test case used throughout this thesis is based on the design of the commercial project at the start of the research project. The commercial design evolved, but for the sake of comparability, only one configuration was used for research.

Figure 3.1(a) shows an artistic rendering of the design of the wPCC design based on a prestudy made by Wallenius Marine. The ship has a length of around 200 m, and a capacity of around 7000 cars. The wings on this rendering are made of a main element with a flap, but were replaced by single element wings, visible in Figure 3.1(b), of the same size and at the same locations. The four wings are placed on the centreline of the ship and have a span of 80 m, a mean chord of 23 m and a NACA 0015 profile all along the span. The wings have an aspect ratio of 3.47, a taper ratio of 0.5 and a total area of 1844 m^2. The rotation axis of the wings are placed at 25% of the chord and the distance between the rotation axis of two consecutive wings is equal to 1.88 times the mean chord.

(a) Hull and wings location.

(b) Wing planform.

Figure 3.1: Artistic rendering of the wPCC design at the beginning of the research project.

3.2 Vortex Lattice Method

The only numerical tool used in this thesis is based on a simple, low-fidelity method. A Vortex Lattice Method (VLM) code is based on potential flow theory but enables to calculate the three dimensional effects that are typically present on a wing, which 2D methods cannot capture. The VLM code is based on the theory from Katz and Plotkin [31] and was first implemented by Helmstad and Larsson [26]. The code was modified to allow an easy integration of multiple wings in various locations with respect to each other.

The basic principle of the VLM method is to discretise the geometry of the wing in a number of panels that follow the shape of the mean chord line and cover the whole span, as shown in Figure 3.2. In this case, since the wing is symmetric, the mean chord line is simply a straight line. The panels are associated with vortex ring elements, consisting of four vortex lines which have the same dimensions as the panels, but are offset in the chordwise direction such that the leading vortex is located at 25% of the chord of the panel from the leading edge of the panel, and the trailing vortex is therefore placed at 25% of the chord of the panel immediately downstream. In Figure 3.2, the blue points show the end points of the vortex lines. The strength of the vortices is unknown, and their calculation is the core of the VLM method. The strength of the vortices is calculated at a collocation point, located at mid span and at three-quarter chord of the panel, by ensuring that there is no flow through the surface at this point. The Kutta condition imposes zero circulation at the trailing edge of the wing. This condition is satisfied by adding one extra row of vortex rings after the trailing edge of the wing, whose intensity is the same as the trailing edge vortices and that extend far downstream, as shown by the red panels in Figure 3.2.

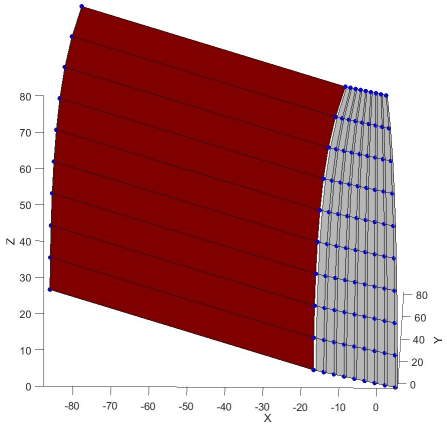

Figure 3.2: Example of the discretisation of one wing with 8 panels in the chordwise direction and 9 spanwise. Figure taken from [38].

This method was chosen because it allows to estimate the 3D effects and the wing interaction effects while running very rapidly on a normal computer. One configuration with four wings could run in about one second on a standard laptop. The VLM code was used in [38] and [33] in comparison with other rapid numerical methods and with more complex 3D CFD for validation. The results compare well, showing the usability of the method to capture wing interaction effects. However, because it is based on potential flow, the stall of the wing cannot be detected, thus limiting the possibility to use the code for trimming optimisation. For this reason, this code was only used shortly and for few publications.

3.3 Wind measurement campaign

The offshore wind measurement campaign, presented in **Paper A** [14] and in [13], was performed on board two sister ships Large Car and Truck Carriers (LCTC) from the Wallenius-Wilhelmsen shipping company, *Figaro* and *Carmen*. They are almost 230 m in length, 32 m in width and can carry more than 7000 car units RT43 [1].

The measurement equipment, visible in Figure 3.3(a), consists in a data acquisition system that records data from three main sensors:

- a continuous wind lidar ZX300M from ZX Lidars® [40],
- an ultrasonic anemometer uSonic-3 Scientific from Metek®,
- an Attitude and Heading Reference System (AHRS) coupled with a Global Navigation Satellite System (GNSS) Ellipse2-N from SBG Systems®.

1 https://walleniuslines.com/wp-content/uploads/2021/12/Figaro_NB4459.pdf

The wind lidar measures the horizontal wind speed and direction as well as the vertical wind speed at twelve different heights, ranging from 10 to 200 m above the deck of the ship, as depicted in Figure 3.3(b), which in this case corresponds to 38 to 228 m above sea level with the ships in loaded condition. The wind is measured sequentially for each height, and the time between two measurements is slightly longer than 1 s, thus leading to a gap of around 15 s between two consecutive measurements at one height.

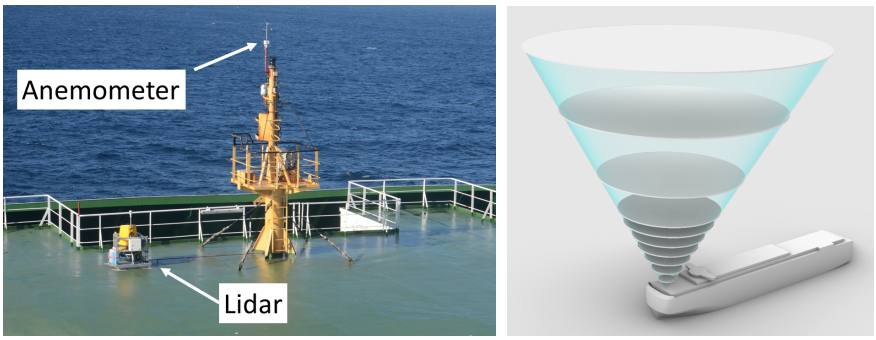

(a) Lidar and anemometer.

(b) Representation of the lidar principle.

Figure 3.3: (a) Picture of the lidar and anemometer installed on *Figaro*. (b) Schematic of the lidar measurement principle. Figures from [13].

The ultrasonic anemometer, placed as high as possible at the bow, as suggested by Yelland et al. [47], also measures the three wind components together with the wind temperature. The sonic anemometer was set to acquire data at the high frequency of 20 Hz to enable the measurement of unsteady effects and fluxes.

The AHRS measures the boat angles (heel and trim), the rotation rates (yaw, roll and pitch) and the accelerations along the longitudinal, transversal and vertical axis and outputs them at a frequency of 5 Hz. The GNSS measures the position as well as the course and speed over ground. All data was output at 5 Hz, the highest possible rate for the GNSS data. The heading of the ship could only be determined by the GNSS because the presence of the steel hull prevents the magnetometer to determine heading, thus the leeway angle of the ship could not be measured and was assumed to be negligible in all data processing.

The lidar measurements stretched over two campaigns, the first on *Figaro*, from the 4th of November until the 13th of December 2019, and the second one on board *Carmen* from the 26th of November 2020 until the 22nd of February 2021, totalling three round-trips across the North-Atlantic Ocean. Figure 3.4 shows the routes followed by the ships where data was successfully collected

according to the post processing procedure described in **Paper A** [14]. Based on this procedure, the total amount of data collected offshore, showed by the black markers in Figure 3.4, corresponds to 27 days, 3 hours and 10 minutes.

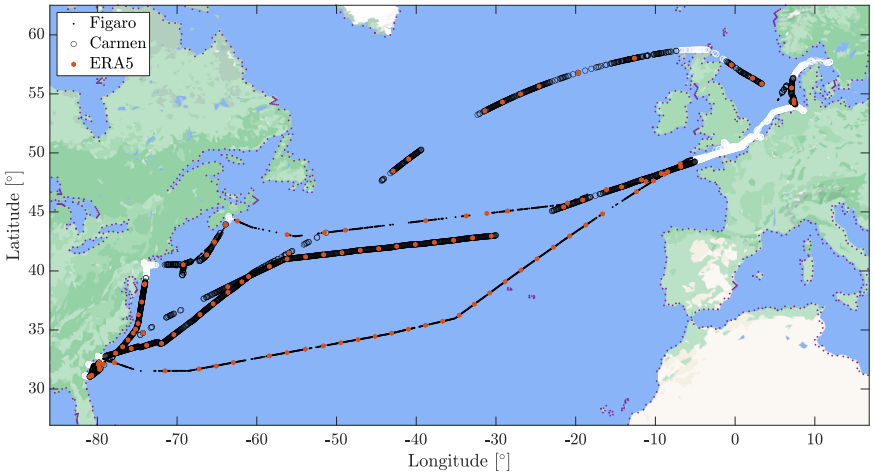

Figure 3.4: Routes of the ships *Figaro* (dots) and *Carmen* (round markers) during the measurement campaigns. The white part of the route is considered close to shore, while the black one is offshore.

3.4 Wind tunnel tests

Wind tunnel tests, dedicated to generating high quality data about multi wing interaction effects, were performed at the R.J. Mitchell wind tunnel of the University of Southampton. Some results are presented in **Paper B**. As depicted in Figure 3.5, the model consisted in three wings, which follow the geometry and relative spacing of the wPCC test case.

Only three wings were tested so that their size could be maximised, while keeping the blockage low. Each wing was mounted on an individual 6-components balance and a rotation mechanism, allowing them to be trimmed separately. The actuation mechanisms were in turn connected to an overall balance on a turntable, measuring the loads globally. On all four balances, the two horizontal forces, as well as the three moments were recorded, but the vertical forces, expected to be negligible, were not considered. The middle wing is also instrumented with 64 pressure taps along three rows located at 33% (22 taps), 60% (22 taps) and 80% (20 taps) of the span, from the root. The pressure was acquired with a MPS4264 pressure scanner from Scanivalve®.

Figure 3.5: Picture of the test setup in the wind tunnel test section, seen from upstream.

The wings are 1.385 m high and have an average chord of 0.4 m. With all wings at 15°, the blockage is only 2.9% of the 3.5 m x 2.4 m cross section of the wind tunnel test section. The tests were conducted with a wind speed of 25 m/s, thus leading to Reynolds number based on the average chord around $0.67 \cdot 10^6$. This value is close to what is typically considered the limit to ensure that the boundary layer is turbulent, but to ascertain that this was the case, strips of zigzag tape were applied on both sides of the wings to force transition to turbulence.

The full test matrix is described in [34]. The results presented in this thesis represent an extract of the test matrix. Apparent wind angles of 15°, 30°, 45°, 60°, 90° and 105°, representative of real conditions for a sailing ship were tested. For each apparent wind angle, a range of variations of trimming angles were tested. In each case, the middle wing stayed at an angle of 0°, 5°, 10°, 15°, 17° and 19°. The front and aft wings were rotated by a series of offsets with respect to the angle of the middle wing. The front wing was rotated by -5°, -2°, -1°, 0°, 1°, 2°, 5°, -2° and 2° while the downstream wing was rotated by 5°, 2°, 1°, 0°, -1°, -2°, -5°, 7° and 2°.

Another series of tests consisted in fixing the wings at given trimming angles and to oscillate the turntable by $\pm 5°$ or $\pm 10°$ around the value of apparent wind angle. These tests simulate the response to a wind gust or oscillations around the course of the ship.

3.5 7 meter test platform

The 7 m test platform, *Christiane*, visible in Figure 3.6, is a 1:30 scale model of the wPCC design, built to be free sailing in open waters. The aim with the platform was twofold; it serves as a demonstrator to showcase what a fully wind powered vessel could look like, with its main purpose being research, to open up new possibilities in terms of model testing. **Paper C**, **D** and **E** are based on experiments performed with the 7 m platform.

Figure 3.6: Picture of the 7 m test platform while sailing in Stockholm's archipelago with one specifically instrumented wing. Photo by Arne Kvarnefalk.

The model is geometrically scaled from the design presented in Section 3.1. As can be seen in Figure 3.6, the wings are however slightly different, because they include 2 steps where the chord and thickness of the profile reduce, to accommodate the possibility to make the wings telescopic. For the experiments presented in **Paper D** and **Paper E**, the rudders were also modified with a span twice as long as the scaled version.

The hull is 7 m long, 1.3 m wide and 1.2 m height of which about 0.9 m constitutes the freeboard. The wings have a span of 2.67 m and a mean chord of 0.75 m. To allow for retractability of the upper sections, the profile varies along the span, with a NACA 0018 at the root and a profile of the same family but with 14.5% thickness at the tip, giving an average section profile close to a NACA 0015.

The boat, practically a robot, contains a network of microcontrollers, actuators and sensors that allow semi-autonomous sailing. A main microcontroller, called the *captain*, receives orders from a tender boat, such as which course to follow, or which experiment to do, and relays the adapted commands to the satellite microcontrollers. A suite of sensors enables to measure the boat motions using an AHRS coupled to a dual antenna GNSS of model Ellipse2-D from SBG Systems®, as well as the wind speed, direction and temperature with several ultrasonic anemometers CV-7 from LCJ Capteurs®. Each wing is actuated independently with its own stepper motor and position sensor.

Apart from the sensors that enable the basic operation of the boat, extra sensors were added to measure aerodynamic characteristics of the wings. For **Paper C** and **Paper D**, differential pressure sensors were added inside the wings to measure the surface pressure. In **Paper C**, 66 sensors were placed in one wing, along 11 strips covering the whole span of the wings. This high density was used to validate the capability of the pressure measurement system. In **Paper D**, all the wings were instrumented with 30 sensors each, along 5 strips located from 5.4% to 87.8% of the span.

For **Paper E**, eight action cameras were mounted at the root of the wings (one camera on each side of each wing), oriented towards the wing's surface in order to record the movement of eleven tell tales that were taped on the surface of the wings. In post processing, a computer vision algorithm was developed to detect the state of the flow (attached of detached flow) at the location of each tell tale.

Chapter 4

Understanding the wind

The wind is the essence of sailing, the fuel that moves sailing ships around. It is so obvious that its complexity is also somehow forgotten and not always accounted for. The physics behind the wind generation is very complex [16], and spans over many different scales, from hundreds of kilometres around the globe all the way down to the wave height or how the sun is shinning. Aerodynamicists typically consider a uniform wind velocity, but the reality is far different. The wind varies with time of course, but with very different time scales. Short wind variations appear in the order of seconds, while weather fronts can change over hours or days. The wind speed and direction also vary with height, forming what is referred to as the Atmospheric Boundary Layer (ABL). The evolution of wind with height and the high frequency wind variations are two important aspects to determine the performance of wind powered vessels, but are not fully understood yet.

4.1 The Marine Atmospheric Boundary Layer

The shape of the Atmospheric Boundary Layer is of paramount importance for performance prediction because it impacts the amount of energy that can be turned into propulsive power. Some models exist to describe the marine ABL, for example in [37] and some experimental data is also available [25, 41, 5], but mostly near shore, which makes it difficult to ensure that the offshore wind in the middle of the ocean would be similar. In an effort to limit this uncertainty, the experimental offshore wind measurement campaign presented in Section 3.3 aimed at collecting wind data in a range of height relevant for wind propulsion.

In **Paper A** [14], we adopted an approach common to the wind energy community to model the evolution of wind speed with height using a power law [25, 27, 46], as

$$U_z = U_{\text{ref}} \left(\frac{z}{z_{\text{ref}}} \right)^{\alpha_{ABL}}, \tag{4.1}$$

with U_z the wind speed at a given height, U_{ref} a reference wind speed at the reference height z_{ref} and α_{ABL}, the power law exponent.[1]

1 In [14], the exponent is denoted α, but to avoid confusion with the angle of attack, denoted α in [11] and [12], it is renamed here.

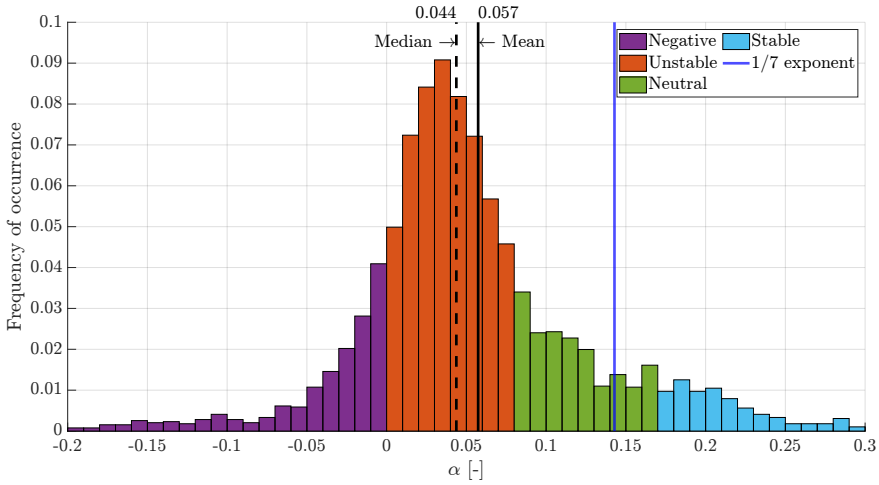

Figure 4.1: Probability distribution of the power law exponent α_{ABL} offshore. From [14].

However, even if the mathematical modelling with a power law is common, determining the value of the exponent α_{ABL} from experiments is done in different ways by different authors; in [14] we used a least square fit of the data at the measurement heights higher than 50 m above the deck, in the form

$$\ln U \;=\; \alpha_{ABL} \ln \frac{z}{z_{\text{ref}}} + C, \tag{4.2}$$

A value of $\alpha_{ABL} = 1/7 \simeq 0.14$ is recommended by most classification societies [29, 2, 15, 8] for the power law exponent and is commonly used in the literature for performance prediction or sea trials processing [44]. The International Towing Tank Committee updated this value to $\alpha_{ABL} = 1/9$ in 2022 [30].

One of the main results from **Paper A** is the presentation of a probability distribution of α_{ABL}, reproduced in Figure 4.1, with the key finding that the most representative value of the power law exponent is $\alpha_{ABL} \simeq 0.035$, very far from the commonly used value of $1/7$.

The distribution presented in Figure 4.1 was only measured over a few months of fall and winter time, nonetheless it compares well with data from [25] that was collected all year round in the North-Sea. The colours represent a distinction of the data based on the stability of the atmosphere; the reader is referred to **Paper A** for the details and the mean values represented in Figure 4.1.

An aspect that is not shown in Figure 4.1 is that the value of α_{ABL} can vary quickly in time. Figure 4.2(a) shows the normalised true wind speed

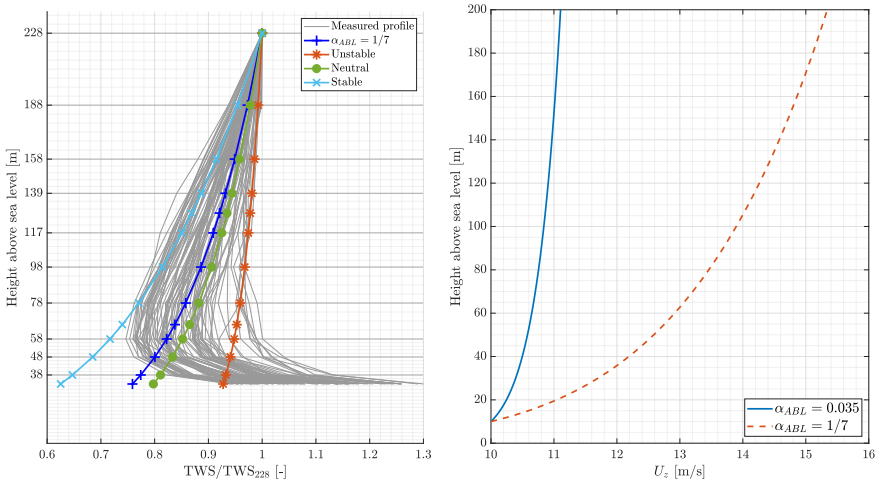

(a) Example ABL profiles measured during one day. Figure modified from [13].

(b) Comparison of the wind speed profiles with $\alpha_{ABL} = 0.035$ and $\alpha_{ABL} = 1/7$.

Figure 4.2: Examples of ABL profiles.

measured during one day on board the ship *Figaro*, together with the different power law profiles obtained in [14]. Almost the whole span of α_{ABL} values is reached throughout the day.

In Figure 4.2(a), the velocity is normalised by the velocity at the highest measurement point, which is not the conventional way of representing a boundary layer. This is done because the value at the highest measurement point is considered the least influenced by the ship. Figure 4.2(b), instead, shows what the vertical wind profile looks like when calculated with $\alpha_{ABL} = 0.035$, shown with the blue solid line, and with $\alpha_{ABL} = 1/7$, shown with the dashed red line, with the a velocity reference $U_{\text{ref}} = 10$ m/s at the reference height $z_{\text{ref}} = 10$ m.

In **Paper A**, an estimation of the differences in terms of kinetic energy between different values of α_{ABL} is presented, and shows that the exponent $\alpha_{ABL} = 1/7$ over predicts the energy by nearly 50% compared to $\alpha_{ABL} = 0.039$ (average value for unstable conditions, see [14]). For the structural design of wind propulsion devices, this excess gives a margin of security, but for performance prediction, this leads to over estimated performance.

Another aspect that affects the performance, is that with a velocity profile that is much closer to uniform, there will be little twist of the apparent wind with height. This should be a rather positive effect, at least for wings, since this means that the top and bottom of the wings have a similar inflow.

4.2 Unsteadiness

Apart from varying with height, the wind varies with time, both in terms of speed and direction. A better understanding of the wind variations is important for the design of control systems for the wind propulsion devices, but could also be important for performance prediction [32].

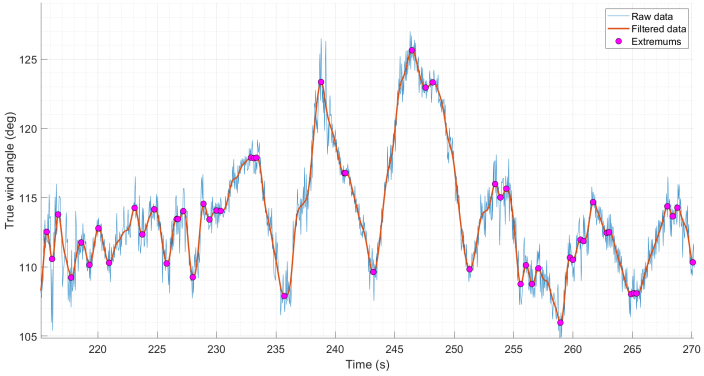

Figure 4.3: Example time series of the true wind angle measured by the ultrasonic anemometer on the ship *Figaro*.

Figure 4.3 shows a time series of the true wind angle measured by the sonic anemometer during the measurement campaign on board the vessel *Figaro* and Figure 4.4 of the apparent wind speed and angle measured by the anemometers at the bow and aft of the 7 m model.

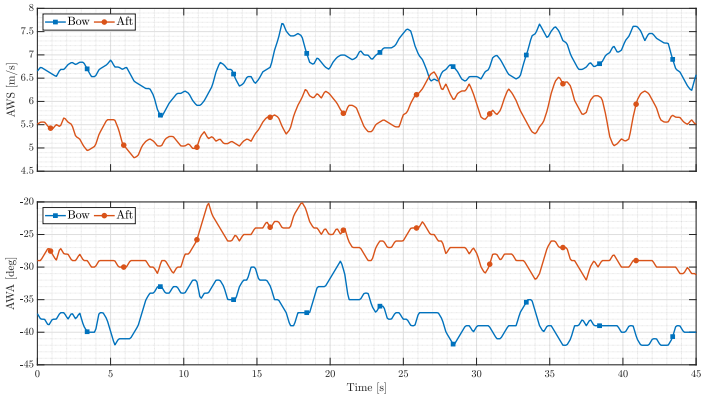

Figure 4.4: Example time series of apparent wind speed and angle measured on the 7 m test platform.

Both Figures 4.3 and 4.4 are specific examples that exhibit large variations of wind angle and speed over short periods of time. Both show variations of wind angle as large as 10 to 15° in only 3 or 4 s. Such large variations are not always happening, but when they do, it will be a challenge for the control systems.

In Figure 4.4, globally, the variations have the same trends, but delays between the front and aft are visible, and some variations are only visible in one of the sensors, highlighting how wind variations are not only temporal but also spatial.

Some temporal wind models exist in the literature, even for representing maritime wind, for example the Frøya wind model by Andersen and Løvseth [3]. An ongoing work using the offshore anemometer data is to recreate a similar wind model and compare it with the one from [3].

Chapter 5

Understanding interaction effects

The interaction effects on a vessel as complex as the wPCC test case are multiple. Both the interactions that appear between the wings and the influence of the hull are of great importance for performance prediction as well as for the development of wing control strategies. While it is possible to separate both effects in simulations or dedicated experiments, in practice on a ship evolving in real environmental conditions, these effects are merged, making their measurement challenging.

The sailing literature does provide some information about sail interaction effects, in particular the interaction between a jib and a main sail [22, 21], but also more recently between multi masted yachts [10]. Some relatively old work exist about experimental assessment of wind powered vessels with multiple wings [7, 28], but only with global force measurements. In [20], results of experiments on a ship with several hybrid wing/soft sails were presented, including load measurement of each wind propulsion unit, however, the sails type and geometry and the vessel are very specific. More recently, [6] performed experiments dedicated to wing-wing interaction effects on two rigid *dynarig* (arc-shaped wing), with varying distance between the wings and different apparent wind angles. Simulation works have been performed with different numerical methods, for example using 3D RANS [36] on a cascade of nine wings, or LES compared with wind tunnel experiments on three wings [35]. Instead of using complex 3D simulations, some authors use 2D simulations and various methods for the vertical integration of the 2D results [43, 33]. All of the studies mentioned here were done in controlled environments or simulation and do not account for unsteady effects. The work presented in this thesis relies on a potential flow panel code, wind tunnel experiments and novel experiments performed with a free-sailing model at sea in unsteady conditions, discussing aspects of wing-wing and wing-hull interactions.

5.1 Wing-wing interaction

In this thesis, the wing-wing interaction effects are studied via three different methods. The numerical panel method was used early on in the project in [38, 33]. In both papers, the VLM method compared well with the 3D CFD simulations, as shown in Figure 5.1.

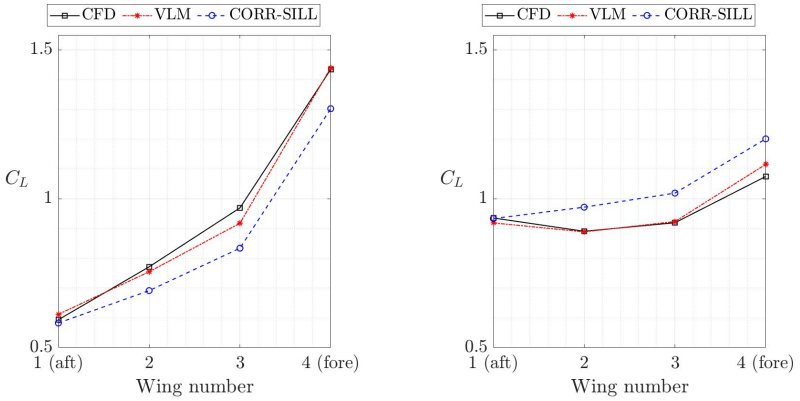

(a) Upwind, 30° apparent wind angle.

(b) Beam reach, 90° apparent wind angle.

Figure 5.1: Lift coefficient with all wings trimmed at 15° angle of attack, obtained with the VLM code and other numerical methods. Figure from [33].

Figure 5.1 also highlights an important interaction effect: when sailing upwind with all wings at the same angle of attack as in 5.1(a), each wing generates less lift than the wing immediately upstream, leading to a large difference between the fore and aft wing. In addition, the front most wing generates higher lift than what the difference between the three other wings would suggest.

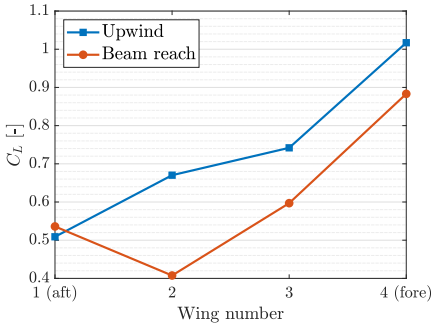

Figure 5.2: Average lift coefficient obtained with the 7 m platform, when sailing on a straight course with all wings set at and angle of attack of 15°.

The same trend is observed in the results presented in **Paper C** and **Paper D**, with data acquired when sailing with the 7 m model. Figure 5.2 shows the average value of the lift coefficient obtained when sailing on

a straight course with all wings trimmed in parallel at 15°, both upwind (blue line with square markers) and on a beam reach (red line with round markers) in the same way was as Figure 5.1, highlighting how the trends are captured by both methods. Figure 5.3 taken from **Paper D**, shows the lift curves obtained when sweeping one wing at a time while keeping the other wings at the same target angle of attack of 15°, while sailing upwind in (a) and on a beam reach in (b).

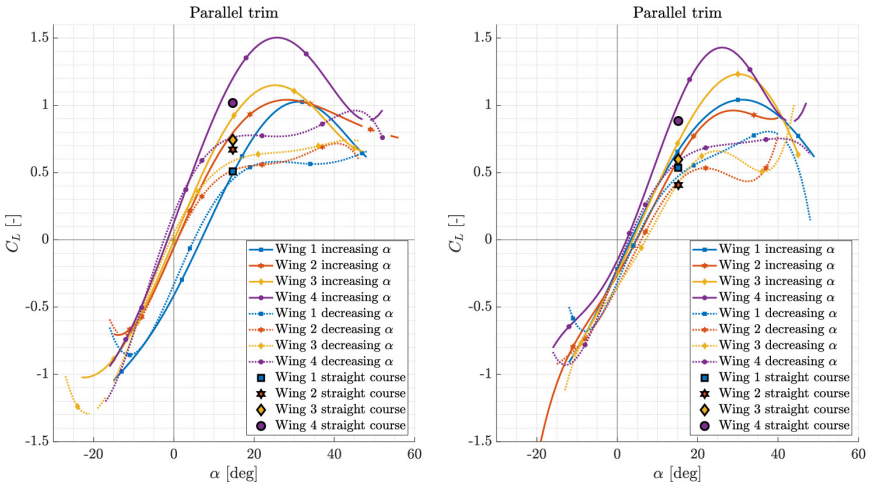

(a) Upwind sailing (b) Beam reach

Figure 5.3: Lift coefficient curves obtained with the 7 m test platform when sweeping one wing while sailing on a straight course, with the other wings trimmed at 15° angle of attack.

From the wind tunnel experiments of **Paper B**, Figure 5.4 shows the lift coefficient for each wing when all wings are set to an angle of attack of 10° and the apparent wind angle is varied from 15° to 90° on the left plot, and on the right, the total thrust and side force coefficients are represented. Similarly to the previous figures, upwind, up to an apparent wind angle of 60°, the aft wing generates the smallest lift, the front one generates the most, and the difference between front and middle is larger than between middle and aft.

The three methods presented here, although very different from all perspectives show consistently the same behaviour of the wings when sailing upwind: the front most wing generates the largest lift and benefits most from the interaction effects, while the downstream wings generate lower lift. Based on Figure 5.4, it is even possible to conclude that the front wing produces higher lift than if the wing was alone, while the two downstream ones generate less than one wing alone.

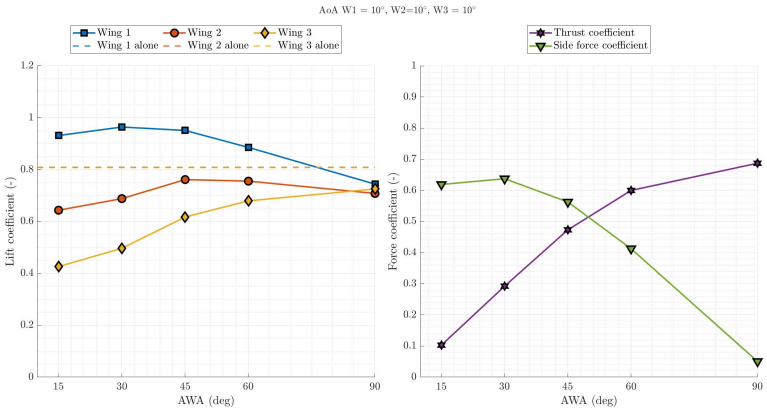

Figure 5.4: Lift coefficient of the three wings for varying apparent wind angle (left) and thrust and side force coefficients (right), obtained in the wind tunnel experiments. Figure from [34].

Looking at the beam reach case, the results from Figures 5.1(b) and 5.2 are consistent: the front wing still generates more lift than the other three, but also the aft wing is not the lowest anymore and is instead more or less at the same level as wing 3, and the smallest lift is generated by wing 2. The relative lift levels are also the same between the two methods: the front wing clearly produces lower lift on a beam reach than upwind, but the other three remain at similar levels. A similar case in the wind tunnel experiments, from Figure 5.4 shows a less clear conclusion: here all wings produce the same amount of lift, the differences are too small to conclude anything about one wing producing more or less lift, but the trend is still the same: the front wing produces sensibly less lift than upwind while the two other have values close to the ones at an apparent wind angle of 45°.

Finally, another aspect of wing-wing interaction that is visible on the right part of Figure 5.4, is that despite the higher lift coefficients upwind than on a beam reach, the thrust coefficient is higher at an apparent wind angle of 90° because the direction of the force is more favourable than upwind.

5.2 The influence of the hull

The influence of the hull on the flow is complicated to asses, first of all because it depends largely on the exact hull shape, on the location of interest along the ship and on the apparent wind angle [47]. Some aspects of the direct influence on the hull are visible in the lidar wind measurements. In Figure 4.2(a), the lower parts of the measured wind profiles diverge largely

from the power law representation, indicating the influence of the hull on the inflow. **Paper A** discusses this influence more in details, but Figure 5.5 shows some of these results.

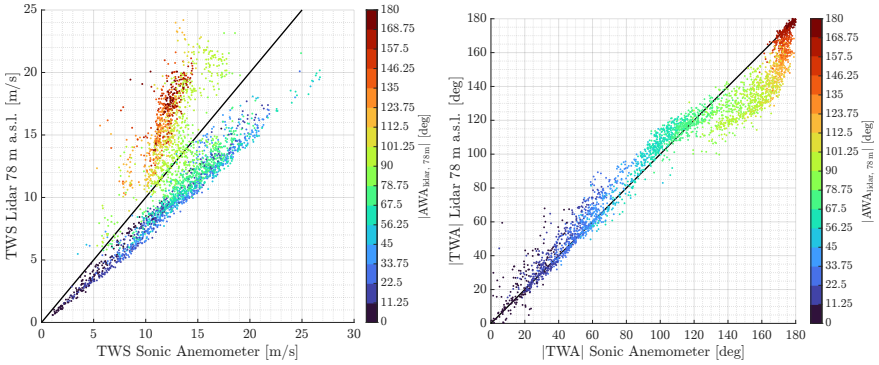

(a) TWS (b) TWA

Figure 5.5: Correlation between the true wind measured by the sonic anemometer and by the lidar 50 m above the deck. Figures from [14].

Figure 5.5 shows the correlation between the true wind measured by the anemometer and the lidar at 50 m above deck, which is considered as the first lidar measurement height where the hull influence is not present anymore. Figure 5.5(a) shows that the anemometer over predicts the wind speed with an almost constant factor, except when the apparent wind angle is higher than around 100°, where the anemometer largely under predicts the true wind speed. Figure 5.5(b) shows that in the same range of apparent wind angles, the true wind angle is also wrongly measured by the anemometer, while below an apparent wind angle of 90°, both lidar and anemometer agree fairly well.

Another example of the hull influence was shown in Figure 4.4, where an example time series of the apparent wind angle and speed from the 7 m model was shown for the anemometers at the bow and stern of the boat. The times series present a clear offset between the measurements at the bow and the aft, both in terms of wind speed and angle. In this case, the boat is sailing upwind and the aft anemometer records a smaller wind speed and an angle about 15° closer to the wind than the bow. This example highlights the combined effects of the hull and the wing interaction, and solely based on these measurements it is not possible to separate one effect from the other.

Finally, Figure 5.6 taken from **Paper B**, shows another aspect of the hull influence, where the deck shape has a direct influence on the flow at the wing root. Figure 5.6(a) shows a wing at an angle of attack around 25°

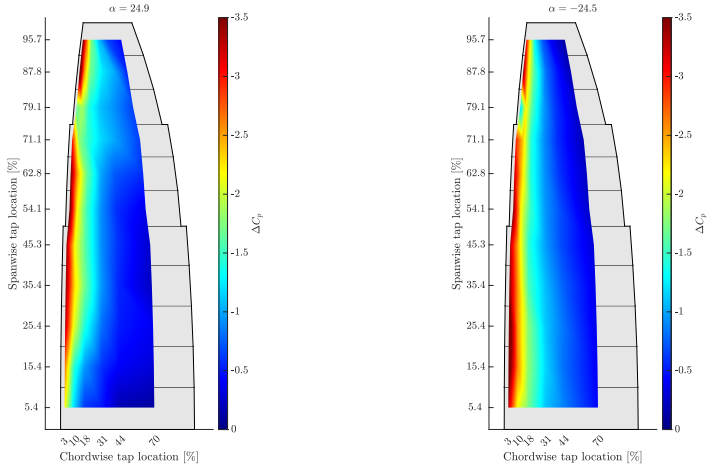

(a) Beam reach

(b) Upwind

Figure 5.6: Map of the pressure difference coefficient for an angle of attack around 25°, when sailing on a beam reach (a) and upwind (b). Figures from [11].

with $\beta_{aw} = 90°$ and Figure 5.6(b) shows the same angle of attack but with $\beta_{aw} = 45°$. The suction peak extends all the way to the root in 5.6(b), but stops somewhere around 15% or the span in 5.6(a).

There are two possible explanations for this difference. When sailing on a beam reach in Figure 5.6(a), most of the wing root is not directly above the deck of the model, while when sailing upwind in Figure 5.6(b), the deck is flat and right below the root of the wind, preventing a root vortex to form, thus leading to higher lift generated by the wing at the root. The other possible explanation is that, despite the rounded corner of the deck, the flow could be be separating from the deck at this angle, leading to a recirculation zone at the root of the wing, as is the case with a hull with sharp corners [45].

Chapter 6

Efficient multi wing trimming when sailing in unsteady conditions

Only when combining the effects described in Chapters 4 and 5 can optimal multi wing trimming be achieved, although the definition of optimality could be a topic of discussion by itself. Instead of affirming to find an optimum, several experiments were performed in this thesis to asses the impact of *efficient* trimming.

Based on the results from Chapter 5 and previous studies from the literature [7, 20], it is clear that, upwind, the interaction effects reduce the performance of the downstream wings. Considering the downwash of the upstream wings, the local angle of attack of a downstream wing is effectively lower than the one of the upstream wing, thus in order to maximise the force, the wings downstream need to be trimmed with higher angles of attack, in a gradual manner. Using the 7 m test platform, in **Paper D**, a series of experiments with the angles of attack gradually increasing were performed. Figure 6.1 shows the results of such gradual trimming, with three starting angle of attack of $10°$, $12.5°$ and $15°$. At iteration 0 all wings have this same angle of attack and at iteration 5, the aft most wing is trimmed with an angle of attack $15°$ higher than the front one, which remains at the starting angle of attack throughout the experiment.

The details of the figure are presented in [12]; the important results here are that the maximum speed (VMG) is reached from iterations 2 or 3 in the middle of the figure, although the lift coefficient keeps increasing when the aft wings are trimmed higher. In the right part of the plot, all wings are stalled or at least partially, and the speed does not vary, contrary to the heeling angle which tends to increase. With this way of relative trimming between the wings, it seems that an optimal trimming would be around $\alpha_{w4} = 12.5°$, $\alpha_{w3} = 15.5°$, $\alpha_{w2} = 18.5°$ and $\alpha_{w1} = 21.5°$, corresponding to iteration 3 in the middle. Trimming the wings to higher angles of attack does not result in better performance. The values from this example are not to be taken as absolute, the aim is to show the impact of the trimming strategy and how and efficient trimming involves many parameters.

In another attempt to measure the impact of gradual trimming with the 7 m model, some of the measurements done for **Paper D** included times when the basic trimming of the sail was gradual, with the following angles

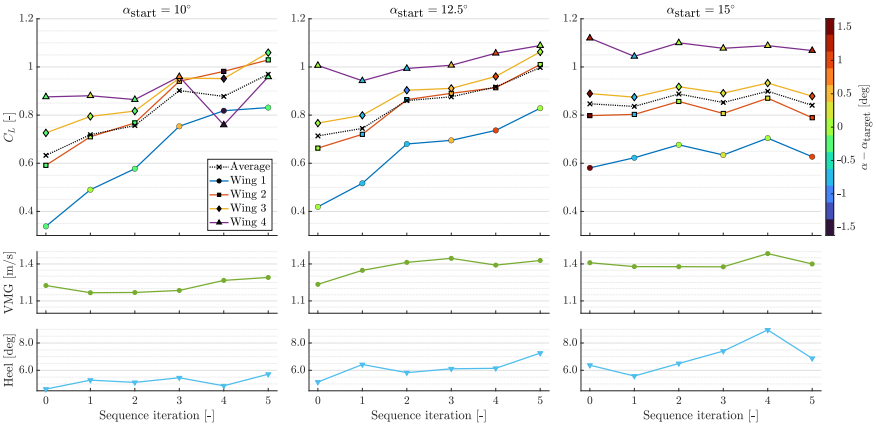

Figure 6.1: Sequential gradual trimming experiments on the 7 m test platform when sailing upwind. Figure from [12].

of attack, $\alpha_{w4} = 15°$, $\alpha_{w3} = 18°$, $\alpha_{w2} = 21°$ and $\alpha_{w1} = 24°$ from fore to aft. Figure 6.2 presents, in the same way as in Figure 5.2, the average lift coefficient obtained when sailing on a straight course with the parallel and the gradual trimming, for the upwind case 6.2(a) and the beam reach case 6.2(b), and shows how much the lift coefficient can be increased by gradual trimming. The gain showed here is quite significant even though the trimming strategy was based on a guess from the author of the thesis and not from an actual optimisation process.

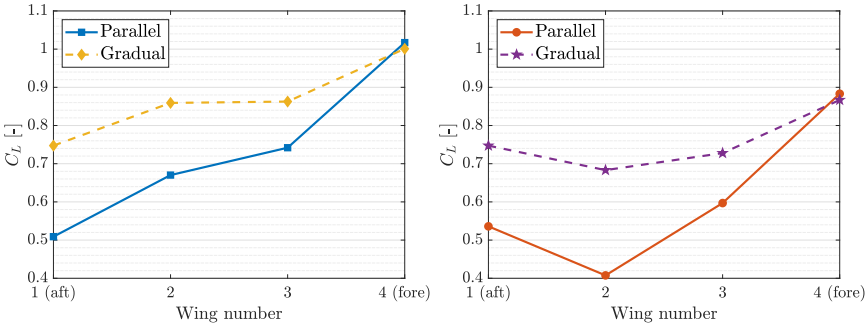

(a) Upwind (b) Beam reach

Figure 6.2: Average lift coefficient when sailing on a straight course with two different trimming strategies.

During the wind tunnel experiments presented in **Paper B**, the variations of trimming angles indicated that with an apparent wind angle of 45°, the maximum lift was obtained with the front wing set 2° lower and the aft wing 7° higher than the middle wing for small angles of attack of the middle wing. The overall maximum thrust was instead obtained with the wings at an angle of attack of 14°, 15° and 16° from fore to aft respectively, with a thrust coefficient $C_x = 0.66$. When all wings were trimmed in parallel with 15° angle of attack, the thrust coefficient was $C_x = 0.56$.

These two configurations were tested when the apparent wind angle oscillates $\pm 5°$ around its initial position, in an attempt to mimic the effects of wind gusts. Figure 6.3 shows the overall thrust coefficient and the lift coefficients of each wing throughout the oscillation when all wings are set to 15°. Figure 6.4 shows the same result but for the gradual trimming.

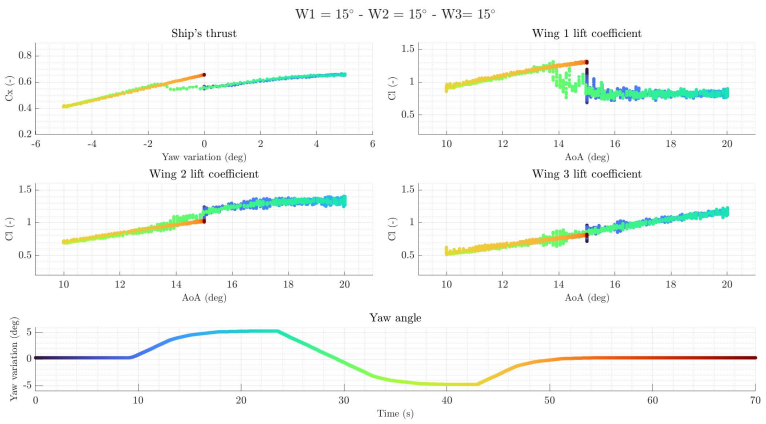

Figure 6.3: Oscillation around apparent wind angle 45° with all wings set at 15° angle of attack in the wind tunnel.

A first result from Figure 6.3 is that, at the beginning, the front wing is stalled, as highlighted by the rapid oscillations of the lift coefficient. When the apparent wind angle reduces by about 1.5°, the flow reattaches on wing 1. At the end, when the apparent wind angle is again 45°, the thrust coefficient if much higher, about 0.65, than at the start due to the reattachment of wing 1. This value is comparable to the maximum overall thrust coefficient obtained with a gradual trimming. In Figure 6.4, no stall is happening on any of the wings, and the start and end values of lift and thrust coefficients are the same. The difference between these two cases highlights why unsteady effects are of paramount importance to find efficient trimming strategies. Both trimming angles here can reach the same value of thrust coefficient,

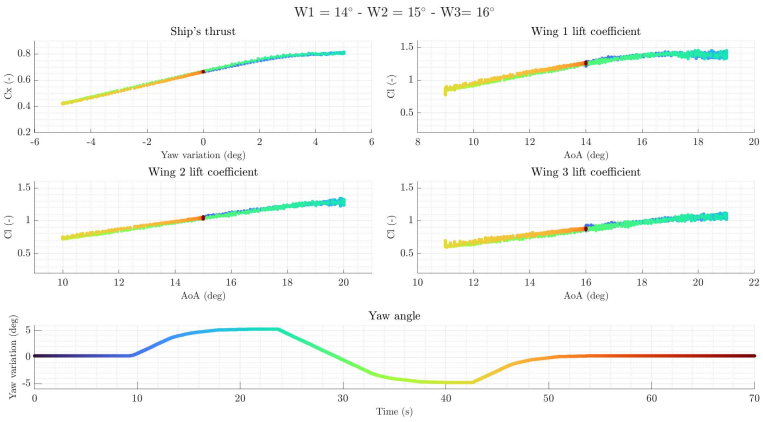

Figure 6.4: Oscillation around apparent wind angle 45° with the wings at an angle of attack of 14°, 15° and 16° from fore to aft, in the wind tunnel.

but the parallel trimming is at risk that one wing could stall, leading to a large loss of thrust. The gradual trimming instead shows little effect of the wind direction variation, which is favourable for efficient trimming.

In addition to wind variations, a ship in real conditions is also experiencing motions due to the environment, which causes another source of unsteadiness to the force generation by the wings, which has already been observed in the sailing literature [19, 23]. A major difference with these studies is that a cargo vessel such as the wPCC has a very different response to waves than a sailing yacht, leading to quite different dynamics.

An important finding from **Paper C** which was also observed in **Paper D** is that when sailing on a straight course, because of the combined impact of all unsteadiness and the fact that the wings are subject to stall hysteresis, an "effective" lift curve appears, which lies somewhere in between the curves obtained before and after stall. Figure 6.5, taken from **Paper C** shows the "effective" lift curve (yellow dashed line) together with the curves obtained by increasing (blue plain curve) and decreasing (red dashed line) the angle of attack. In **Paper D**, the results were confirmed and showed to happen regardless of the trimming strategy.

This "effective" lift curve is particularly difficult to interpret because it encompasses several unsteady effects at the same time and is also linked to the presence of stall hysteresis. In full-scale, the boat motions will be slower and smaller, thus their impact is likely to be less important, and it is also uncertain if the hysteresis effects will be present with the high Reynolds number that the wings will have in full-scale. Nonetheless, this

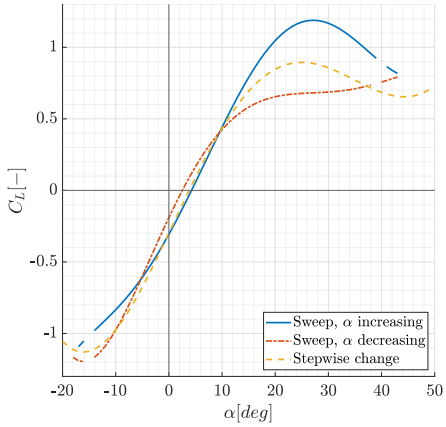

Figure 6.5: Lift curves obtained by increasing the angle of attack in steps and sailing on a straight course between each step, when sailing upwind. Figure from [11].

result draws the attention to the need of accounting for unsteady effects for performance prediction. Kjellberg et al. [32] presented a numerical study of unsteady effects using the wPCC test case which combines a spatio-temporal wind model and the response of the ship to waves. Even though the aerodynamic model is quasi-static and cannot predict hysteresis effects, one of their conclusions points to the importance to account for unsteady effects for performance prediction.

Chapter 7

Conclusions

7.1 Discussion

The work presented in this thesis spans a wide variety of methods. Ranging from one of the simplest potential flow-based simulation code to a complex ad hoc free sailing model; from wind tunnel tests to wind measurements 200 m above sea level in the middle of the Atlantic. Ranging from a few seconds runtime to months of data gathering and preparation; from low-fidelity to real-life measurements. These methods could hardly be more different from one another, and yet, in the previous chapters, they were combined; some compared well; some could only describe parts of the problem and other encompassed all aspects. If they do compare well, some might ask, which should be used? The answer is simple: all of them. The problems at stake are complex and involve many different scales, many different physical phenomena which are not easy to solve or whose effects are difficult to separate.

Low fidelity numerical methods are the only way to explore the design space and give an overview of the possibilities.

Wind tunnel testing is needed to ensure that the low fidelity models are not far off, and in the final design stages it is the only method that can capture most of the physics.

Real-life measurements are needed when the other methods cannot measure at the locations of interest, such as in the middle of the ocean.

When model testing in uncontrolled environment, not all physics can be extrapolated to full-scale, that is a fact, and yet, it is the only way to combine the interaction effects between the wings, the impact of the hull, the influence of the wind variations and the impact of boat motions without any modelling.

It was not used in this thesis, but also Computational Fluid Dynamics has a role to play here. By implementing a full-scale, 3D, aero and hydrodynamic unsteady model that includes the Atmospheric Boundary Layer, waves and hysteresis effects? Certainly not, unless maybe it also makes coffee, but seriously, such “do-it-all” model is nearly impossible to make, would be almost impossible to validate and would not be possible to run in a realistic time. However, simulations can help understand the physical phenomena better,

can deliver high fidelity results with variations that would be impractical to do in experiments. Once CFD models are validated with experimental results, they can be used to explore the design space further.

From the point of view of the methodology, this thesis aims at showing that there is no “one-size-fits-all” method, and that the new challenges created by the development of wind propulsion call for a myriad of methods, experiments and simulation codes to be developed in order to fully grasp all important aspects of the problem.

7.2 Future work

The experiments presented in this thesis are quite extensive, but the results only cover parts of the collected data, which need to be explored further.

Based on the findings of this thesis, many useful “bricks” are available to optimise multi wing trimming strategies and implement algorithms for vessel control systems. Such new algorithms can be tested in real conditions on the 7 m test platform.

Most of the topics discussed in this thesis are still partially unknown and should be explored further. The interaction effects can be well captured by many simulation methods, but some effects are still difficult to understand. The impact of the hull is clearly measured both in full scale and model scale, but there is a lack of simple methods to estimate these effects on different hull shapes or at varying locations. Those are only some examples and the list could be extended further.

An important aspect that has been touched upon on several scales in this thesis is the difficulty to measure relevant quantities in real conditions. Measuring the wind profile without the impact of the hull is difficult; measuring the pressure at the surface is possible, but how to ensure that rain or the boat motion doesn’t affect the measurements; how to know if the pressure variation comes from a change in wind or because of trimming? Those are just examples of difficulties in measuring aerodynamic quantities in a meaningful way, and could lead to many more research questions.

Chapter 8

Summary of the appended papers and contribution to the field

Paper A: Observation of the Atmospheric Boundary Layer over the Atlantic and its effects for wind propulsion

Paper A presents measurements of the wind field at sea, in the North-Atlantic Ocean, at heights relevant for wind propulsion from a ship in commercial operation, using a wind lidar. To the best of our knowledge, this has never been done before for the purpose of wind propulsion. Wind measurements from ships were not new, but most of the existing studies are about meteorological aspects, thus with measurement heights much higher than those at which wind powered ships will evolve.

The main findings of **Paper A** concern two aspects of importance for the performance prediction of wind powered vessels as well as for the development of control strategies for the wind propulsion units. One part discusses the shape of the vertical wind speed profile and its modelling using a power law. We show a probability distribution of the power law exponent and conclude that the typical value from the literature, $1/7 \simeq 0.14$, is very far from the observed reality, where the most representative value is around 0.035. For the same reference wind speed, the exponent 1/7 over predicts the amount of kinetic energy of the wind by around 50%.

The second aspect that **Paper A** discusses is the influence of the hull on the surrounding flow field. The wind field is affected as high as one to tow times the hull height above the deck, meaning that most of the existing wind propulsion unit technologies will evolve in a very perturbed flow. In extreme cases, the wind angle was measured to rotate by 15° to 20° in the first 15 m above the deck. These results depend largely on the exact hull shape, but they highlight the importance of accounting for the hull presence for performance prediction. They also emphasise how the placement, and calibration, of the on-board sensors on the ship is crucial to determine the real wind conditions while sailing, which would greatly influence control algorithms.

Paper B: Multi-wing sails interaction effects

Paper B presents preliminary results from wind tunnel experiments dedicated to the understanding of wing-wing interaction effects. The experiments were carried out at the R.J. Mitchell wind tunnel of the University of Southampton. In order to maximise the Reynolds number, the model size was maximised, which led to the testing of only three wings instead of the four used in the rest of the research project. The Reynolds number was around 0.67 million which should be high enough to ensure a turbulent boundary layer, thus ensuring that the results were as close as possible to full-scale. At the time of the experiments, to the best of our knowledge, this was the only wind tunnel tests with more than two wings with such high Reynolds number.

The main objective of the experiments was to provide high quality data for validation of numerical methods, but also to increase the understanding of wing-wing interaction effects. The results emphasised how the interaction when sailing upwind is driven by the downwash and upwash of one wing onto the other, leading to the upstream wing generating more lift than the one immediately downstream, regardless of the trimming strategy. Some asymmetric trimming strategies were also tested and proved surprisingly efficient in some cases, highlighting the complexity of the interaction effects. Finally, the results also showed the potential impact of stall hysteresis, where the same wing configuration can lead to very different thrust coefficients depending on the history of the flow. An example is shown where the total thrust coefficient is reduced by 25% when the fore wing is stalled and not the other.

Paper B was written very shortly after the experiments, and could only scratch the surface of the dataset, Unfortunately, for practical reasons, the authors have not yet been able to publish an in-depth study, so the scientific contribution of the experiments is still to be expended.

Paper C & D: Unsteady pressure measurements at sea on the rigid wings of a model wind propelled ship.

Paper C and **D** were written as a two parts paper because they rely on the same experimental asset: the 7 m test platform developed at KTH Royal Institute of Technology and its pressure measurement system. **Paper C** presents the development and testing of the pressure measurement system, focusing on proving its abilities. **Paper D** focuses on the measurement of wing-wing and wing-hull interaction effects and of unsteady effects in real conditions.

An important scientific contributions of **Paper C** and **Paper D** comes from the uniqueness of measuring aerodynamic aspects in a real environment, accounting for all interaction effects. The 7 m test platform allows for a mix between model testing and full-scale measurement in an uncontrolled environment. Similar work has been done by the sailing research community on full-scale leisure yachts, but this is a new type of testing for wind propulsion.

Part A: Measurement system development.

Paper C focuses on the development of the pressure measurement system, the description of the 7 m test platform and on the specific way that this type of model testing in an uncontrolled environment is performed to yield good quality results.

The results show the ability of the system to measure the effects under investigation, but also showed novel results about the aerodynamic behaviour of the wings in an unsteady environment. By sweeping the wings dynamically, lift curves with stall hysteresis, typical for such thick profiles, are measured. When varying the angle of attack, but keeping it fixed for a while, however, an "effective" lift curve appears, with values more or less in-between the curves from the pre- and post-stall cases. This has a large implication for performance prediction, since the effective lift curve is about 25% lower than what steady numerical or experimental methods would predict.

Part B: *in-situ* aerodynamic performance measurements.

Paper D is about the *in-situ* measurements of aerodynamic performance of a model of a wind powered vessel. Some of the experiments focused on the measurement of the different interaction effects, wing-wing and wing-hull, while others where aimed at evaluating the performance of a gradual trimming strategy, as opposed to a parallel trimming with all wings at the same angle.

Although the method differs largely from the rest of the literature about interaction effects, some results from **Paper D** agree well with others from numerical or wind tunnel studies. Some results on the other hand are more surprising and bring new perspectives to the understanding of interaction effects, when accounting for the hull and unsteadiness. Such result is for example the lift coefficients when sailing on a beam reach, with the wind coming about 90° form the side, and the wings parallel. In **Paper B**, all wings produced the same amount of lift, while in **Paper D**, we showed that the fore wing still produces significantly more lift, and that the aft wing produced more lift than the one directly in front.

Paper E: Evaluation of the flow state over a rigid wing-sail through tell-tale detection using computer vision

Paper E presents a method to determine the flow state on a rigid wing based on filming tell tales and a computer vision algorithm. **Paper E** introduces the "attached flow ratio" as a measure of what percentage of the flow is attached or detached on the wing. Although the algorithm is based on a simple logic which requires very little processing power and no algorithm training, **Paper E** shows that the main aerodynamic characteristics can be measured, for example the stall hysteresis discussed in **Paper C** and **Paper D** is clearly visible in the value of the attached flow ratio when dynamically sweeping the wings.

The method presented in **Paper E** could easily be used for a full scale wing prototype, thus enabling to get the main aerodynamic characteristics of a wing without modifying it and with very little instrumentation.

Appendix A

List of supervised student projects

The following presents a list of the student projects (bachelor thesis, master's thesis, internship or projects) that I supervised or co-supervised during my PhD. They are all related to our sailing research, and some of these works led to publications or helped us in the research project.

Regardless how successful the projects ended up, I would like to thank all the students for their help, but also for what I learned by supervising them. I knew I enjoyed supervising, but I didn't expect to learn so much from doing it.

- 2019, Valérie Bouysses, *Rig Performance Evaluation for Wind Powered Pure Car Carrier*, Master's thesis
- 2020, Clara Nermark & Katja Nordström, *Modellbygge av framtida seglande lastfartyg*, Bachelor thesis
- 2020, Alexis Aurdren de Kerdrel, *Treatment of experimental data on the atmospheric boundary layer over sea*, Internship
- 2021, Daniel Workinn, *A high-level interface for a sailing vessel*, Bachelor thesis
- 2021, Suzanne Herzog, *Performance analysis of a wind powered car carrier model*, Internship
- 2021, Corentin Paret, *Performance analysis of a wind powered car carrier model*, Internship
- 2021, Arne Kvarnefalk & Oskar Rosbarve, *Mätning av rigglaster på segelbåten Christiane*, Bachelor thesis
- 2022, Antonia Hillenbrand, *Experimental Investigation of the Aerodynamics of a Sailing Cargo Vessel with Four Rigid Wingsails under Unsteady Sailing Conditions*, Master's thesis
- 2022, Marcus Olivecrona & Edvin Hagberg, *Bättre kurskontroll-och styregenskaper för Project Oceanbirds experimentbåt*, Bachelor thesis

- 2022, Benjamin Sitbon, *Système de communication entre contrôleurs*, Internship
- 2022, Cynthia El Khoury, *A camera solution and algorithm for telltales*, Internship
- 2023, Rebecca Martinson & Elliot Collin *Generation of Realistic Time Series for Open Sea Wind*, Project
- 2024, Hanna Andrae, *The Design and Construction of a Boundary Layer Rake for Measuring Boundary Layers in Subsonic Wind Tunnels*, Research Academy for Young Scientists (RAYS) project
- 2024, Nicolas Dubeau, *Étude, design et construction d'une maquette de soufflerie d'un navire à voile*, Internship

References

[1] Albert E. Abbott Ira H.and von Doenhoff. *Theory of Wing Sections: Including a Summary of Airfoil Data*. Dover Publications, 1959.

[2] American Bureau of Shipping. *Guide For Wind Assisted Propulsion System Installation*. 2020.

[3] Odd Jan Andersen and Jørgen Løvseth. "The Frøya database and maritime boundary layer wind description". In: *Marine Structures* 19.2 (2006). DOI: 10.1016/j.marstruc.2006.07.003.

[4] John David Anderson. *Fundamentals of Aerodynamics*. Second edition. McGraw-Hill, 1991. Chap. 1.

[5] Cristina L. Archer, Brian A. Colle, Dana L. Veron, Fabrice Veron, and Matthew J. Sienkiewicz. "On the predominance of unstable atmospheric conditions in the marine boundary layer offshore of the U.S. northeastern coast". In: *Journal of Geophysical Research: Atmospheres* 121.15 (2016), pp. 8869–8885. DOI: 10.1002/2016JD024896.

[6] Giovanni Bordogna, Jan Alexander Keuning, Rene H.M. Huijsmans, and Marco Belloli. "Wind-tunnel experiments on the aerodynamic interaction between two rigid sails used for wind-assisted propulsion". In: *International Shipbuilding Progress* 65 (2018), pp. 93–125. DOI: 10.3233/ISP-180143.

[7] William Michael Spenser Bradbury. "Large Sailing Ships - A Fluid Dynamic Investigation". PhD thesis. Imperial College London, 1983.

[8] Bureau Veritas. *Wind Propulsion Systems*. Rule Note NR 206 DT R01 E. 2021.

[9] NASA Glenn Research Center. *Beginners guide to Aeronautics*. https://www1.grc.nasa.gov/beginners-guide-to-aeronautics/. Accessed August 2024.

[10] Vincent Chapin, Romaric Neyhousser, Guillaume Dulliand, and Patrick Chassaing. "Analysis, Design and Optimization of Navier-Stokes Flows around Interacting Sails". In: *MDY06 International Symposium on Yacht Design and Production*. 2006.

[11] Ulysse Dhomé, Antonia Hillenbrand, Jakob Kuttenkeuler, and Niklas Rolleberg. "Unsteady pressure measurements at sea on the rigid wings of a model wind propelled ship. Part A: Measurement system development." In: *Ocean Engineering* (2024). Submitted.

[12] Ulysse Dhomé, Antonia Hillenbrand, Jakob Kuttenkeuler, and Niklas Rolleberg. "Unsteady pressure measurements at sea on the rigid wings of a model wind propelled ship. Part B: *in-situ* aerodynamic performance measurements." In: *Ocean Engineering* (2024). Submitted.

[13] Ulysse Dhomé, Jakob Kuttenkeuler, Mikael Razola, and Antonio Segalini. "Preliminary results on measurements of the atmospheric boundary layer over the Atlantic." In: *Innov'sail 2020, The 5th International Conference on Innovation in High Performance Sailing Yachts and Sail-Assisted Ship Propulsion (INNOV'Sail 2020)*. Gothenburg, Sweden. Online, 2020.

[14] Ulysse Dhomé, Jakob Kuttenkeuler, and Antonio Segalini. "Observation of the atmospheric boundary layer over the Atlantic and its effects for wind propulsion". In: *Journal of Wind Engineering and Industrial Aerodynamic* (2024). submitted.

[15] DNV. *Environmental conditions and environmental loads*. Recommended Practice DNV-RP-C205. 2021.

[16] Stefan Emeis. *Wind Energy Meteorology - Atmospheric Physics for Wind Power Generation*. Springer Cham, 2018. DOI: 10.1007/978-3-319-72859-9.

[17] Jasper Faber, et. al. *Fourth IMO GHG Study 2020*. International Maritime Organisation. URL: https://www.imo.org/en/OurWork/Environment/Pages/Fourth-IMO-Greenhouse-Gas-Study-2020.aspx.

[18] Fabio Fossati. *Aero- Hydrodynamics and the performance of sailing yachts*. Adlard Coles Nautical, 2009.

[19] Fabio Fossati and Sara Muggiasca. "Experimental Investigation of Sail Aerodynamic Behavior in Dynamic Conditions". In: *Journal of Sailboat Technology* 2.8 (2011), pp. 1–41. URL: https://onepetro.org/JST/article-pdf/2/8/1/642648/sname-jsbt-2011-02.pdf.

[20] Toshifumi Fujiwara, Grant E. Hearn, Fumitoshi Kitamura, and Michio Ueno. "Sail–sail and sail–hull interaction effects of hybrid-sail assisted bulk carrier". In: *Journal of Marine Science and Technology* 10 (2005), pp. 82–95. DOI: 10.1007/s00773-005-0191-4.

[21] Arvel Gentry. "A Review of Mordern Sail Theory". In: *Proceedings of the eleventh AIAA Symposium on the Aero/Hydronautics of Sailing*. 1981.

[22] Arvel Gentry. "The Aerodynamics of Sail Interaction". In: *Proceedings of the third AIAA Symposium on the Aero/Hydronautics of Sailing*. 1971.

[23] Frederik C. Gerhardt, Richard G. J. Flay, and Peter Richards. "Unsteady aerodynamics of two interacting yacht sails in two-dimensional potential flow". In: *Journal of Fluid Mechanics* 668 (2011). DOI: 10.1017/S0022112010004842.

[24] Heikki Hansen, Karsten Hochkirch, and Uwe Hollenbach. "Wind Propulsion Performance Prediction Impact on Bulk Carrier Business Case". In: *8th High Performance Yacht Design Conference (HPYD 8)*. 2024.

[25] Charlotte B. Hasager, Detlef Stein, Michael Courtney, Alfredo Peña, Torben Mikkelsen, Matthew Stickland, and Andrew Oldroyd. "Hub Height Ocean Winds over the North Sea Observed by the NORSEWInD Lidar Array: Measuring Techniques, Quality Control and Data Management". In: *Remote Sensing* 5.9 (2013), pp. 4280–4303. DOI: 10.3390/rs5094280.

[26] Aron Helmstad and Tomas Larsson. "An Aeroelastic Implementation for Yacht Sails and Rigs." Master's thesis. KTH Royal Institute of Technology, 2013.

[27] Shih-Ang. Hsu, Eric A. Meindl, and David B. Gilhousen. "Determining the Power-Law Wind-Profile Exponent under Near-Neutral Stability Conditions at Sea". In: *Journal of Applied Meteorology and Climatology* 33.6 (1994), pp. 757–765. DOI: 10.1175/1520-0450(1994)033<0757:DTPLWP>2.0.CO;2.

[28] Peter Ingham and Ole Tersløv. "Wind Tunnel Tests and Manoeuvre Simulator Tests With Different Types of Sails and Ships". In: *Journal of Wind Engineering and Industrial Aerodynamics* 20 (1985), pp. 169–185. DOI: 10.1016/0167-6105(85)90017-0.

[29] ITTC. *Analysis of Speed/Power Trial Data*. International Towing Tank Conference. Recommended Procedures and Guidelines 7.5-04-01-01.2, Revision 01. 2014.

[30] ITTC. *Preparation, Conduct and Analysis of Speed/Power Trials*. International Towing Tank Conference. Recommended Procedures and Guidelines 7.5-04-01-01.1, Revision 07. 2022.

[31] Joseph Katz and Allen Plotkin. *Low-speed aerodynamics: from wing theory to panel methods*. Ed. by McGraw-Hill. Cambridge University Press, 1991.

[32] Martin Kjellberg, Frederik Gerhardt, and Sofia Werner. "Sailing Performance of Wind-Powered Cargo Vessel in Unsteady Conditions". In: *Journal of Sailing Technology* 8.01 (Dec. 2023), pp. 218–254. DOI: 10.5957/jst/2023.8.12.218.

[33] Karolina Malmek, Ulysse Dhomé, Lars Larsson, Sofia Werner, Jonas W. Ringsberg, and Christian Finnsgard. "Comparison of two rapid numerical methods for predicting the performance of multiple rigid wingsails". In: *The 5th International Conference on Innovation in High Performance Sailing Yachts and Sail-Assisted Ship Propulsion (INNOV'Sail 2020)*. Gothenburg, Sweden. Online, 2020.

[34] Laura Marimon Giovannetti, Ulysse Dhomé, Karolina Malmek, Adam Persson, and Chiara Wielgosz. "Multi-Wing Sails Interaction Effects". In: *SNAME 24th Chesapeake Sailing Yacht Symposium, CSYS*. June 2022. DOI: 10.5957/CSYS-2022-006.

[35] Takuji Nakashima, Yoshihiro Yamashita, Yasunori Nihei, and Qiao Li. "A Basic Study For Propulsive Performance Prediction of a Cascade of Wing Sails Considering Their Aerodynamic Interaction". In: *International Ocean and Polar Engineering Conference*. June 2011. URL: https://onepetro.org/ISOPEIOPEC/proceedings-pdf/ISOPE11/All-ISOPE11/ISOPE-I-11-451/1670065/isope-i-11-451.pdf.

[36] Kazuyuki Ouchi, Kiyoshi Uzawa, and Akihiro Kanai. "Huge Hard Wing Sails for the Propulsor of Next Generation Sailing Vessel". In: *Second International Symposium on Marine Propulsors, Hamburg, Germany*. 2011. URL: https://api.semanticscholar.org/CorpusID:67767920.

[37] Alfredo Peña, Sven-Erik Gryning, and Charlotte B.Hasager. "Measurements and Modelling of the Wind Speed Profile in the Marine Atmospheric Boundary Layer". In: *Boundary Layer Meteorology* 229 (2008), pp. 479–495. DOI: 10.1007/s10546-008-9323-9.

[38] Adam Persson, Da-Qing. Li, Fredrik Olsson, Sofia Werner, and Ulysse Dhomé. "Performance prediction of wind propulsion systems using 3D CFD and route simulation". In: *Transactions of RINA, Wind Propulsion Conference* (2019).

[39] Loyd's Register. *Energy Efficiency Retrofit Report 2024: Applying wind-assisted propulsion to ships*. 2024. URL: https://www.lr.org/en/knowledge/research-reports/applying-wind-assisted-propulsion-to-ships/.

[40] Anthony Rutherford, Mark Pitter, Chris Slinger, Edward Burin des Roziers, Will Barker, and Michael Harris. "The effect of motion on continuous wave lidar wind measurements". In: *Windpower 2013*. 2013.

[41] Johannes Schulz-Stellenfleth, Stefan Emeis, Martin Dörenkämper, Jens Bange, Beatriz Cañadillas, Thomas Neumann, Jörge Schneemann, Ines Weber, Kjell zum Berge, Andreas Platis, Bughsin' Djath, Julia Gottschall, Lukas Vollmer, Thomas Rausch, Mares Barekzai, Johannes Hammel, Gerald Steinfeld, and Astrid Lampert. "Coastal impacts on offshore wind farms - a review focussing on the German Bight area". In: *Meteorologische Zeitschrift* 31.4 (Oct. 2022), pp. 289–315. DOI: 10.1127/metz/2022/1109.

[42] Ignė Stalmokaitė, Tommy Larsson Segerlind, and Johanna Yliskylä-Peuralahti. "Revival of wind-powered shipping: Comparing the early-stage innovation process of an incumbent and a newcomer firm". In: *Business Strategy and the Environment* 32.2 (2023), pp. 958–975. DOI: 10.1002/bse.3084.

[43] Ignazio Maria Viola, Matthieu Sacher, Jinsong Xu, and Fei Wang. "A numerical method for the design of ships with wind-assisted propulsion". In: *Ocean Engineering* 105 (2015), pp. 33–42. DOI: 10.1016/j.oceaneng.2015.06.009.

[44] Sofia Werner, Jonny Nisbet, Axel Hörteborn, and Rasmus Nielsen. "Speed Trial Verification for a Wind Assisted Ship". In: *RINA Wind Propulsion Conference*. London, United Kingdom, Sept. 2021.

[45] Chiara Wielgosz, Laura Marimon Giovannetti, Sofia Werner, and Jakob Kuttenkeuler. "CFD Study on the Different Stratifications of the Atmospheric Boundary Layer and their Effect on the Performance of Wind Propelled Ships". In: *8th High Performance Yacht Design Conference (HPYD 8)*. 2024.

[46] Bowen Yan, Qiusheng Li, Pak Wai Chan, Yuncheng He, and Zhenru Shu. "Characterising wind shear exponents in the offshore area using Lidar measurements". In: *Applied Ocean Research* 127 (2022). DOI: 10.1016/j.apor.2022.103293.

[47] Margaret J. Yelland, Bengamin I. Moat, Robin W. Pascal, and David I. Berry. "CFD Model Estimates of the Airflow Distortion over Research Ships and the Impact on Momentum Flux Measurements". In: *Journal of Atmospheric and Oceanic Technology* 19.10 (2002), pp. 1477–1499. DOI: 10.1175/1520-0426(2002)019<1477:CMEOTA>2.0.CO;2.